2015

MULTI-INSTRUMENTAL INVESTIGATION OF VOLCANIC OUTGASSING AT PACAYA VOLCANO, GUATEMALA.

Carlo Prandi
Michigan Technological University, cmprandi@mtu.edu

MULTI-INSTRUMENTAL INVESTIGATION OF VOLCANIC OUTGASSING AT PACAYA VOLCANO, GUATEMALA.

By

Carlo Maria Prandi

A THESIS

Submitted in partial fulfillment of the requirements for the degree of

MASTER OF SCIENCE

In Geology

MICHIGAN TECHNOLOGICAL UNIVERSITY

2015

This thesis has been approved in partial fulfillment of the requirements for the Degree of MASTER OF SCIENCE in Geology.

Department of Geological and Mining Engineering and Sciences

Thesis Co-Advisor: *Gregory P. Waite*

Thesis Co-Advisor: *Chad Deering*

Committee Member: *Claudia Corazzato*

Department Chair: *John S. Gierke.*

Table of Contents

1) Abstract

Pacaya is one of the most active volcano in the world and it is only ≈30Km South of Guatemala City, the capital of Guatemala, that has a population of about 2 million of people and a surrounding metropolitan area where ≈4.5 million of people live. So mitigate the volcanic hazard improving the knowledge and the understanding of Pacaya is fundamental to decrease the risk factor at which the surrounding population is exposed. This study aims to furnish a new large database, the analysis, the comparison and the interpretations of data that come from different techniques of sampling, about the volcanic outgassing at Pacaya.

A total number of 440 samples were collected with the CO_2 accumulation chamber, principally from the northern side of the volcano; about 8000 images were obtained using an UV camera from the foot of Pacaya and about two weeks of seismological data were collected by a seismic station buried nearby the summit of the volcano. The processing of all these data produced the first CO_2 efflux map and the first comparison between SO_2 data and seismic data of this volcano; furthermore it gave back to us the emission rate values for both the volcanic gasses. Moreover we mapped a new possible system of faults, in this work called "secondary faults", and, using Google Earth Pro, the opening of a new eruptive fissure on the South-Eastern side of the volcano. We also confirmed the NNW orientation of the magma ascension and that there is a direct relationship between low-frequencies seismic signal and the outgassing of the SO_2.

In the last chapter of this study we propose a list of much food for thought for future studies and also solutions and ideas to solve them.

2) Introduction

After 200 years of repose Pacaya resumed activity in 1961; since then it has been one of the most active volcanoes of Central America. The activity is primarily Strombolian and produces tephra falls, ballistic bombs, and lava flows which are relatively dangerous for the people that live in the area that surround the volcano. The biggest risk for the surrounding communities is represented by a possible failure of the new volcanic cone (Mackenney Cone) (Eggers, 1971; 1983; Vallance et al. 1995; Rose et al., 2013; Schaefer et al., 2013).

Despite this premise, the number of studies about this volcano remains small and the knowledge limited. In particular there are no published studies of the volcanic outgassing after the big eruption of the 2010, so we decided to address this with new information that comes the combination of three different instruments:

- A portable diffuse flux-meter made by West System S.r.l.
- A SO_2 camera Alta U6 made by Apogee Instruments Inc and equipped with a JENOPTIK's CoastalOpt 105mm UV-VIS SLR Lens and an Andover Optics Corp.
- Short-period seismic systems: Mark Products/Sercel 3-component L-22 sensors with a natural frequency of 2 Hz and a sensitivity of 88 V/m/s and RefTek 130 recorders.

From Pacaya's outgassing studies we obtained information about the volcanic activity and about the geological features that are present underneath the surface. These structural information are particularly important for a better knowledge on how the magma's ascent and the regional fields of stresses interact and a better idea on how these factors can result into a future collapse of the new volcanic cone.

In this work we present a geological description of the investigated area; a report of the fieldwork campaign; a chapter that contains the description of the principles and methodologies of the techniques used for this study; the results obtained with the associated discussion; some conclusions; and a chapter where we reported the recommendations for future works on this volcano.

3) Background

a) Regional geologic setting

Pacaya is an active compound stratovolcano located in the Central America Volcanic Arc, ~30km south of Guatemala City, that reaches a maximum elevation of ~2500 m above sea level (a.s.l.). Along with Fuego and Santiaguito, the other two open-vent volcanoes in Guatemala, Pacaya is part of the volcanic front associated with the subduction of the Cocos plate underneath the Caribbean plate. (Franco et al., 2010; Matías Gomez et al., 2012; Schafer et al., 2013; Rose et al., 2013).

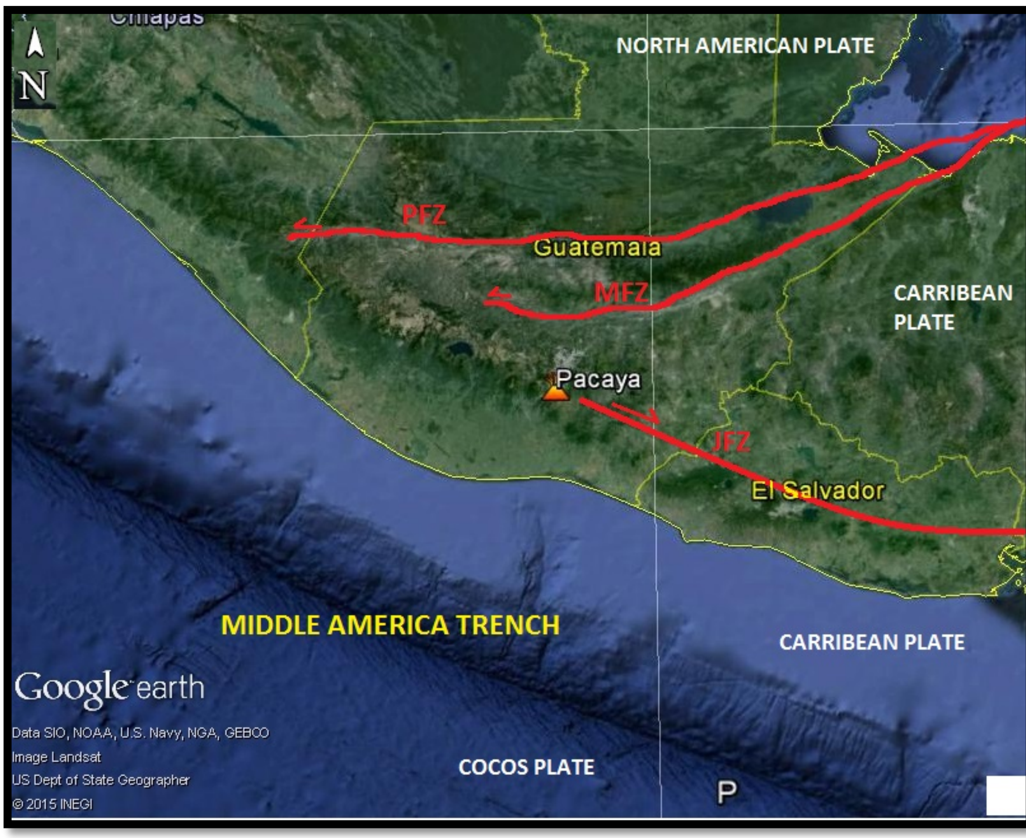

Figure 1- Location of the Pacaya volcano and main structural features. The Motagua (MFZ), the Polochìc (PFZ) and the Jalpatagua faults zone (JFZ) are shown as red lines (modified from Google Earth. See the Appendix for documentation of permission to use this material).

The area is located south of the Motagua and Polochic faults system that is considered the left-lateral transform boundary between the Caribbean plate and North America plate (Guzman-Speziale, 2001; Schafer et al., 2013). This regional tectonic setting is characterized as an extensional regime, which forms a series of north-striking grabens in the region. The Guatemala City graben is presently the most active and absorbs most of the E–W extensional deformation. Moreover a right-lateral fault zone named Jalpatagua fault zone interacts with the Pacaya's regional stress field (Carr 1976; Guzman-Speziale, 2001; Franco et al. 2010; Schafer et al., 2013). The location of this fault zone is not perfectly defined, but it can be approximated using the geological maps of the area like those showed in the works of Eggers (1972) and Carr (1976); in particular Carr, 1976 has shown that this fault zone and others right-lateral fault zones are near and nearly parallel to active volcanoes, probably because the magma's upwelling created zones of weakness in the crust (Eggers, 1972; Carr, 1976).

b) Local geologic setting and evolution of the complex volcano

An additional system of faults adds more local complexity to the tectonic framework of Pacaya, in fact the complex has grown on the southern rim of the Amatitlàn caldera. This caldera is located 10km south of Guatemala City and it has a diameter of 16-14km (Fig. 2). The caldera's most active period was between ~300,000 years to ~23,000 years before present with a total erupted volume of more than 70km^3 of volcanic products. Amatitlàn caldera is evidenced by gravity data, geological observations, circumferential faults, hot springs and well-logs of the area rocks. These data suggest that the caldera is active and probably will erupt in the future (Wunderman & Rose, 1984). The volcanism of the Amatitlàn quadrangle is divided into four eruptive phases which characterize the evolution of Pacaya: (1) growth of a small andesitic stratovolcano, now much eroded, disrupted by faulting and landslides and covered by pyroclastic deposits; (2) A strong basaltic eruptive phase that formed the initial cone about 0.5Ma; (3) an extrusive andesite-dacitic phase that emplaced domes as "Cerro Chiquito" and "Cerro Grande" ~0.16Ma, during this phase, between 600 and 1500 yr B.P., the south-western sector collapsed leaving a "horseshoe-shaped" caldera; (4) development of the modern complex composed of six cones including Cerro Grande, Cerro Chiquito, Cerro Chino, Pacaya Viejo, Pacaya, and Cerro Mackenney (Eggers, 1971; Bardintzeff and Deniel, 1992; Conway,1992; Kitamura and Gómez, 1995; Vallance et al. 1995; Matías Gomez et al., 2012).

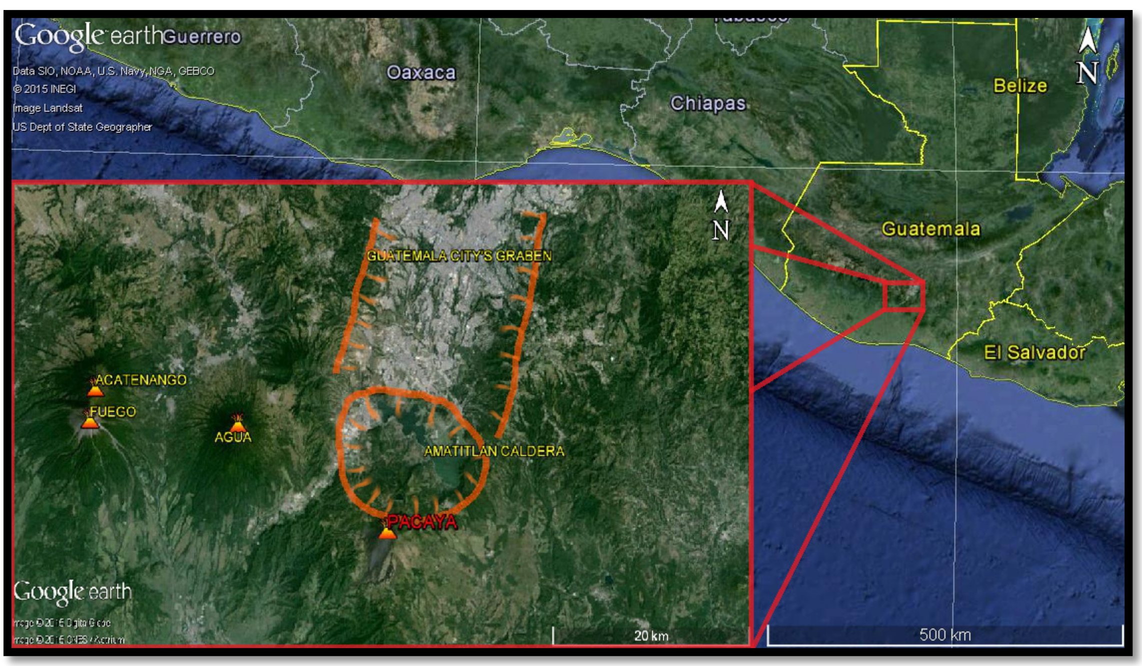

Figure 2- Location of the Amatitlàn caldera and the Guatemala City's graben (map source: Google Earth. See the Appendix for documentation of permission to use this material). The orange lines indicate the borders of the Amatitlàn caldera and the Guatemala City's graben (Wunderman and Rose, 1984)

The latest phase of volcanism, which continues today, is marked by several eruptive events that typically last for 100 to 300yr and repose periods which are generally 300-500yr long. The latest historical eruptions are dated 1585yr B.P., from ca. 1651 to 1678yr B.P. and 1775yr B.P., in this last event "Cerro Chino" was mainly formed (Eggers, 1971; Conway, 1992). In summary, Pacaya is a volcanic complex formed by the overlapping of several basaltic cones and it has and age of several thousand years (Rose et al. 2013).

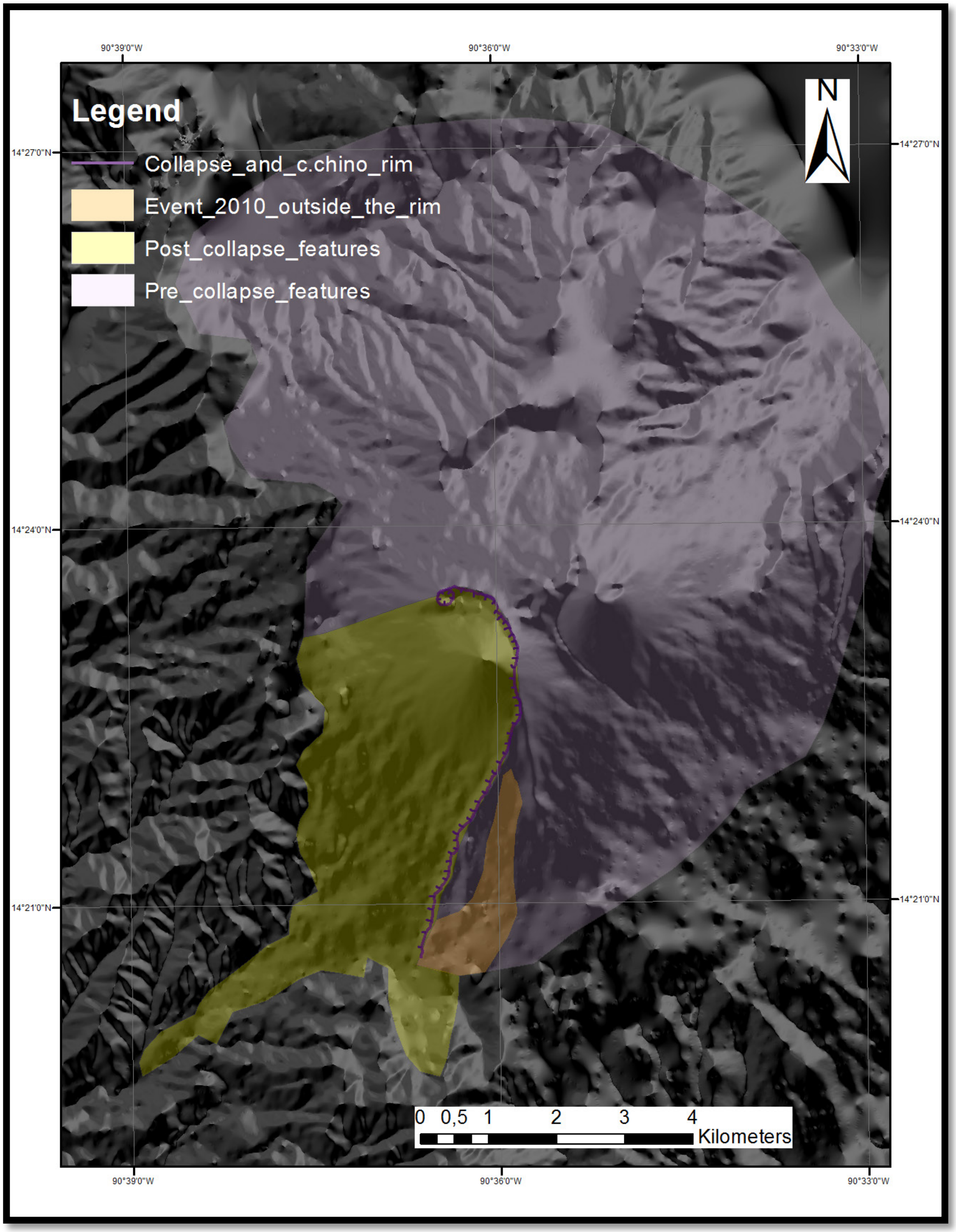

Figure 3- Simplified map of recent Pacaya volcano eruptive features.

c) *Current activity*

The current eruptive period at Pacaya began in 1961. Matías Gomez et al. (2012) mapped 349 vents and 263 eruptive units (249 of these are lava flows and the remainder are: pyroclastic flows deposits, alluvial deposits, eolian sediments, spatter and air-fall units) deposited between 2012 and 2010. The eruptive style varies from purely effusive to Hawaiian and Strombolian (lava fountains and moderated explosions). The most energetic eruption culminated on 21 May 2010 and produced a 21km high ash column, which covered the down-wind areas with an estimated ash volume of 1.3×10^7 m^3. Furthermore, given the very strong wind of that day, some ballistics reached distances up to ~4 km to the north of Pacaya damaging several villages (Wardman et al., 2012). During this particular eruptive event some vents appeared outside the collapse amphitheater. The vents inside the collapse rim are distributed in clusters with the highest concentration at the summit of Mackenney cone. This distribution indicates two principal directions of vent alignments: SW-NE and SSE-NNW. The SSE-NNW alignment connects the 2010 vents with the summit vents and the Cerro Chino (Rose et al., 2013). In addition, Schaefer et al. (2013) have shown, by a morphometric analysis, how this vent orientation of clusters is correlated and justified by the orientation of fissures which follow the regional stress field. The regional ENE direction of the minimum principal stress axis is perpendicular to the volcanic rift, and plane of the ancestral SW collapse. This zone of weakness will likely drive future collapses due to the asymmetric growth of the new volcano.

4) Methods

a) Diffuse soil CO_2 flux

1. Principles

Multiple studies of volcanic areas have shown that the total flux of gas does not entirely come from the summit or active vents, but also diffuses from volcano-tectonic and tectonic features on and around the volcanic edifice. The quantity of diffuse degassing is very important to calculate the total output of gas for a certain area. The accumulation chamber technique has been widely used in order to measure this contribution and to map geological features in volcanic and geothermal areas (Giammanco et al., 1997, 1998; Chiodini et al. 1998, 2001; Frondini et al., 2004; Notsu et al., 2005; Padrón et al. 2008; Melian et al., 2014; Harvey 2015).

A portable diffuse flux-meter made by West System S.r.l. was utilized for this study (Fig. 4). The instrumental setup is composed of: 1) an accumulation chamber (Type B) with an electromechanical mixing device that causes a turbulence in the chamber, 2) a LICOR LI-820 infrared (IR) CO_2 gas analyzer, and 3) a Trimble handheld computer connected to the instrument by a Bluetooth connection that controls the acquisition of data in real time.

The internal volume of the Type B chamber is $6.186*10^{-3}$ m^3, with a base area of $3.140*10^{-2}$ m^2. The pump has a rated flow of 1000 SCCM (standard cubic centimeters per minute); this configuration results in a detection limit of 10 mmol/m^2/day (*Personal communication from Davide Continanza – WestSystem S.r.l.*).

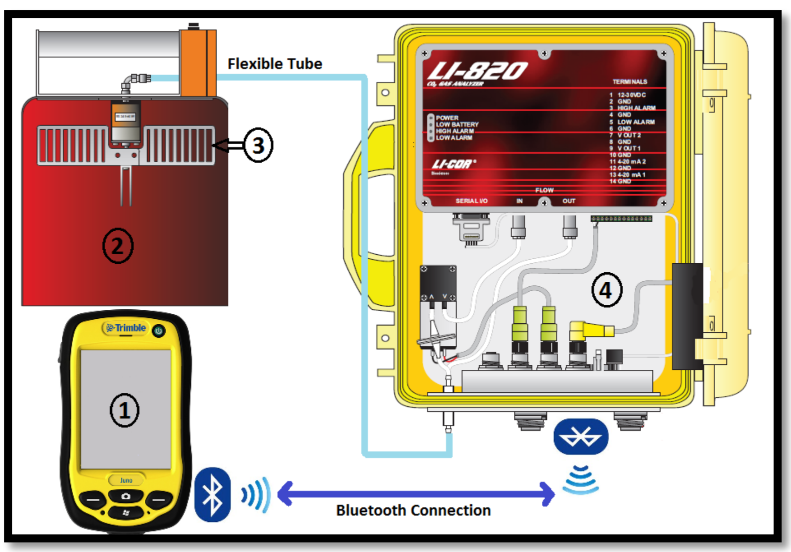

Figure 4 -Illustration of the portable diffuse flux-meter components. 1) Handheld computer by Trimble. 2) Accumulation chamber (type B). 3) Rotor for the air mixing. 4) Hard case that contains a battery, a gas analyzer and a pump (modified from WestSystem S.r.l. Handbook).

2. Analytical procedure

Following the guidelines given by Chiodini et al. (1998) and by the WestSystem S.r.l. the chamber was set on the ground to ensure a tight seal for each measurement. During windy days some fine-grained material was piled around the chamber in order to reduce atmospheric contamination. The air coming from the soil is continuously pumped out from the chamber, sent to the IR spectrometer and then sent back to the chamber in order to avoid drops in the CO_2 concentration. Filters are placed between the chamber and the spectrometers to prevent dust from entering and damaging the IR cell.

The IR spectrometer measures the gas concentration once every second and transmits this measurement through an analog to digital converter for the handheld computer. On this device the user is able to see the increase in CO_2 concentration vs. time in real time. The typical measurement lasts for about two minutes, but when gas flux was low more than five minutes were necessary to reduce the error to acceptable values (regression >0.9). Note that, when the CO_2 flux is close to the limit of detection (low flux values), the ErrQ is always close to zero and it doesn't increase with time.

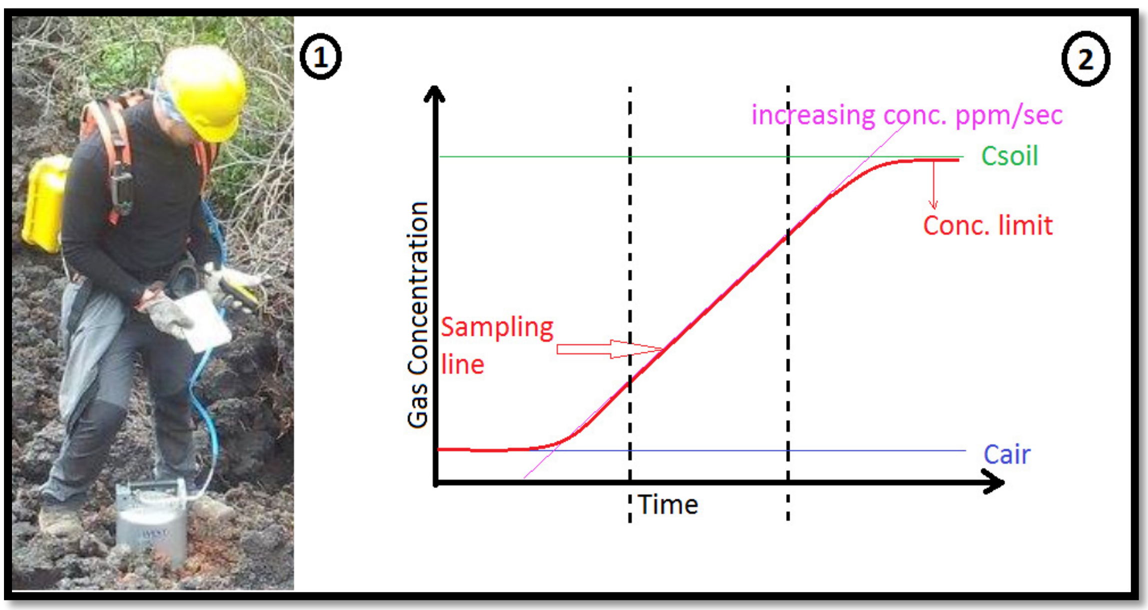

Figure 5- 1) Sampling procedure. 2) Theoretical curve of the gas concentration) Theoretical curve of the gas concentration: CAir is the typical CO_2 concentration in the atmosphere (roughly 350ppm), CSoil is the gas concentration in the soil, "Sampling line cleaning" is the area where the CO_2 from the soil starts to replace the air present in the pump, when the carbon dioxide's concentration become close to the soil concentration the flux curve slope decreases; the two black lines delimit the optimal flux's interval for the calculation of the total flux (modified from WestSystem S.r.l. Handbook).

An attempt was made to keep the spacing between measurements at roughly 55 meters, but the resultant grid is not regularly spaced because some areas are not accessible or too dangerous. In high flux areas the spacing was reduced to less than 10 meters in order to obtain more detailed coverage. In areas where the flux variability was low, nearly zero, the spacing was increased to greater than 60 meters to ensure measurements could be made over the largest possible surface.

3. Data Analysis

The data was processed using the software "FluxRevision" provided by WestSystem S.r.l. to obtain flux value in ppm/s and ppm/m^2/day with an associated ErrQ (Fig. 6).

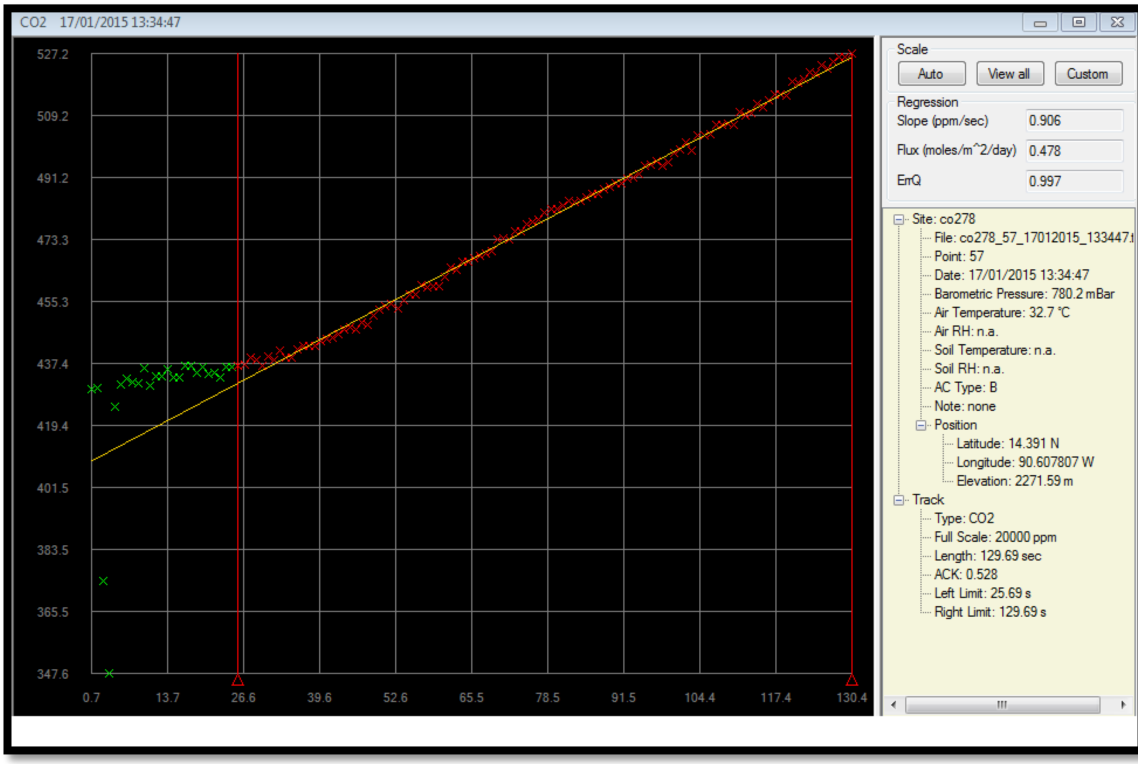

Figure 6- Example of the FluxRevision's interface. On the x-axis is shown the time in seconds, on the y-axis is shown the relative concentration of the CO^2. The yellow line is the regression line that has the best fit with the points' (green and red x) trend. The two vertical lines define the interval with the highest ErrQ.

The values in ppm/s were converted in g/m^2/day using the following equations:

$$1.\quad Fg = Fppm * K * mCO_2$$

Where Fg is the flux value in g/m^2/day, $Fppm$ is the flux value in ppm/s, mCO_2 is the molecular weight of the carbon dioxide (44.01 g/mol) and K is:

$$2.\quad K = \frac{86400 * P}{10^6 * Tk * R} * \frac{V}{A}$$

Where P is the atmospheric pressure in mBar (HPa), V is the volume of the chamber in m^3, Tk is the air temperature expressed in degrees Kelvin, R is the gas constant $8.314*10^{-2}$bar*L/K/mol and A is the chamber inlet net area in m^2. The final calculated flux is given in g/m^2/day.

From these equations it is evident how the barometric pressure and air temperature influence the value of K. These two factors not only influence the *K* value, but Hinkle (1994) has proven how these factors influence the gas flux from the soil. Furthermore, Chiodini et al. (1998) demonstrated experimentally that the atmospheric pressure is inversely proportional to the flux of carbon dioxide from the soil. Both the barometric pressure and the air temperature are automatically recorded by the instrument (e.g. Fig. 6). Some unrealistic or zero value measurements of the barometric pressure were corrected using the data from the INSIVUMEH's weather station that is ≈23km far from the volcano; this is the weather station of the La Aurora International Airport (GUA). These values have been corrected depending on the difference in elevation between the station and the sampling points using the equation:

$$3. \quad Ps = Pgua - (Picao - Pgua)$$

Where:

$$4. \quad Picao = A + B * Pgua$$

Where P_S is the atmospheric pressure at the sample points, *Pgua* is the atmospheric pressure at the La Aurora International Airport's station, *Picao* is the correction value that is obtained multiplying *Pgua* by A and B that are 2 correction factors reported on the Manual of the ICAO Standard Atmosphere (ICAO Doc. 7488) and in the appendix (Table 3).

The values under the limit of detection (LOD) were retained and substituted with a value equal to LOD/√2 based on the methods of Croghan and Egeghy (2003) and Verbovsek (2011), which was shown to be preferable to any other replacement methods (e.g. LOD/2, LOD, zeros or no data).

In order to obtain the total flux output and create flux maps, the raw data were interpolated using a stochastic simulation technique. The sequential Gaussian simulation method (sGs) has been chosen because it can reproduce realistic maps of spatial variability of the flux. Furthermore, it gives an estimated uncertainty useful to calculate the range of the total flux over all the conducted simulations. (Cardellini et al., 2003; Frondini et al., 2004; Padròn et al., 2008; Harvey et al., 2015). The software used for these simulations is GSLIB; the guidelines and steps followed in this phase are meticulously reported in Deutsch and Journel (1998). Knowing the nearest neighbor measured points' spatial position and flux value, the sGs method needs a semi-variogram model in order to correlate, estimate, and model each unknown point of the study area. The semi-variogram model is built on the empirical semi-variogram obtained from the data set. The best way to obtain the optimal input factors to create the semi-variograms is to use geostatistical analyst software. In this study we used the geostatistical analyst tool of ArcGis 10.2. The final output from GSLIB was imported in ArcGis 10.2 in order to obtain a better visualization of the resultant maps and calculate the final flux value for the carbon dioxide.

b) UV camera and seismic data

1. Principles

Since the 1970's SO_2 spectrometers have been largely used to measure the sulfur dioxide emission from active volcanoes (Bluth et al., 2007; Burton et al., 2014), but technology advances have facilitated a new SO_2 monitoring instrument based on digital cameras. A key advantage of UV cameras is that they can quantify the rates of outgassing during the volcanic explosive activity and compare the outgassing data with the acoustic and seismic ones (Mori and Burton, 2006; Dalton et al., 2009; Nadeau et al., 2011; Tamburello et al., 2012; Tamburello et al., 2013; Burton et al., 2014).

In this study was utilized an Alta U6 made by Apogee Instruments Inc equipped with a JENOPTIK's CoastalOpt 105mm UV-VIS SLR Lens and an Andover Optics Corp. bandpass optical filter centered at 307 nm. This camera was connected to a laptop and controlled using the software MaxIm DL. The set up time is in between 10 and 15 minutes. The most important specifics are summarized in the following table (Table 1):

Table 1- specifics of the used UV-Cam

Pixels	1024 x 1024, 16-bit
Exposure Time	20 milliseconds to 183 minutes (2.56 microsecond increments).
Image Sequencing	1-65535 image sequences under software control.
Cooling	Thermoelectric with forced air. Max 50°C below ambient temperature.
Temperature Stability	±0.1° C.
Color corrected	250nm - 650nm.
Manual focus	0.5 m – infinity.
Optical filter	Centered at 307nm.

For the acquisition of the seismic data a seismometer were positioned nearby the summit of Pacaya volcano at ≈180m E from the active vent Fig 8. The seimometer is a short-period Sercel 3-component L-22 with a natural frequency of 2 Hz.

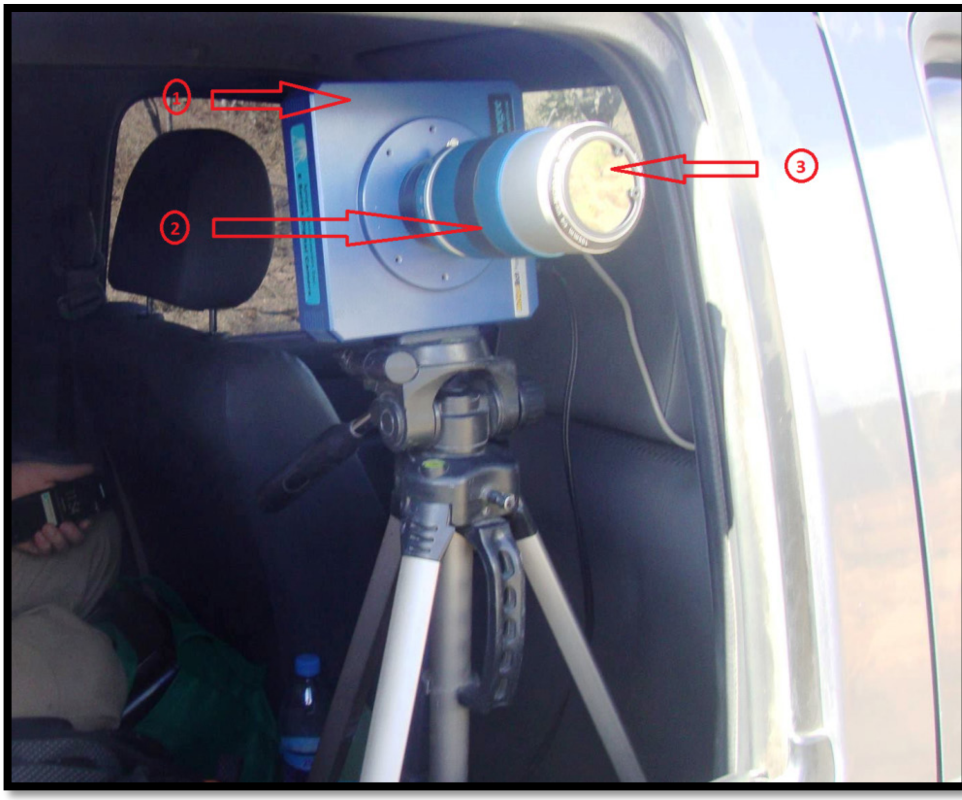

Figure 7- Picture of the UV camera and its components. 1) Alta U6. 2) CoastalOpt 105mm UV-VIS SLR Lens. 3) Andover Optics Corp. bandpass optical filter.

2. Analytical procedure

Following the guidelines given by Bluth et al. (2007), Dalton et al. (2009), Kantzas et al. (2010) and Nadeau (2011) the camera was properly set, cooled and calibrated. The distance from where the UV images were taken during the 19^{th} and the 21^{st} is about 4.5km north of, and ≈900 m below, the summit; whereas during the 20^{th} the distance was about 2.5km and the difference in elevation was ≈1000m (Fig. 8).

Figure 8- Location of the Seismic station and of the 2 acquisition points for the UV cam (modified from Google Earth. See the Appendix for documentation of permission to use this material).

To calibrate the camera, and retrieve SO2 emission rates during the data processing, we used 2 calibration cells that contain a known concentration of SO_2; the two concentrations are 395ppm*m and 1388ppm*m. The calibration process was done every 60 minutes in order to eliminate the differences due to the varying intensity of the light during the day. Both the camera's and the laptop's clocks were synchronized with the UTC time.

The seismometer was installed following the steps described in the PASSCAL installation guide (www.passcal.nmt.edu). The instrument was buried with a GPS timing system (that was synchronized with the UTC time) and its channel number two oriented toward the magnetic north pole using a Brunton compass. The built-in level permitted to orient the instrument in the three dimensions. With the seismometers was buried a RefTek 130 data acquisition system (DAS) with a 18V battery pack in order to supply the energy to the station.

3. Data analysis

The SO_2 data have been processed using the UVCamSO2 suite of programs written by Nadeau (2011) and reported in Nadeau et al. (2014). The program was originally written for Matlab R2008b and it was modified to work with the latest version of Matlab R2014b. The different graphical user interfaces allow to process the digital images in different ways. In fact, the user can display imagery, create AVI files from sequences, derive the plume speed and the emission rate calibrating the program every different subset of images using a background image and an image of the calibration cells. Instead of using background images (images obtained capturing the clear sky) to flatten the pictures, a “dummy image” was created in order to eliminate the effects of vignetting.

Matlab R2014b was also used to process the seismic data. The objective of this analysis was to evaluate any possible relationship between outgassing rate and seismicity. Because most of the seismic signals associated with outgassing are typically in the long-period band (0.5 – 5 Hz; e.g., McNutt, 2005), the data were filtered between 0.5Hz and 5Hz with a two-pole, two-pass Butterworth filter and then visualized them with two real-time seismic amplitude measurements (RSAM) of 10sec and 30sec (Endo and Murray, 1991).

The 10 seconds RSAM showed a better correlation with the UV-camera data so we decided to use those for our comparisons. In order to investigate this correlation between sets of data we interpolated the SO_2 data on the time vector of the RSAM and then we used the “xcorr” command of Matlab to extrapolate the lag (expressed in tens of seconds) that shows the best cross-correlation factor.

Finally the seismic and the SO_2 data have been plotted together in order to compare them following the Nadeau et al. (2011) example (Fig. 9).

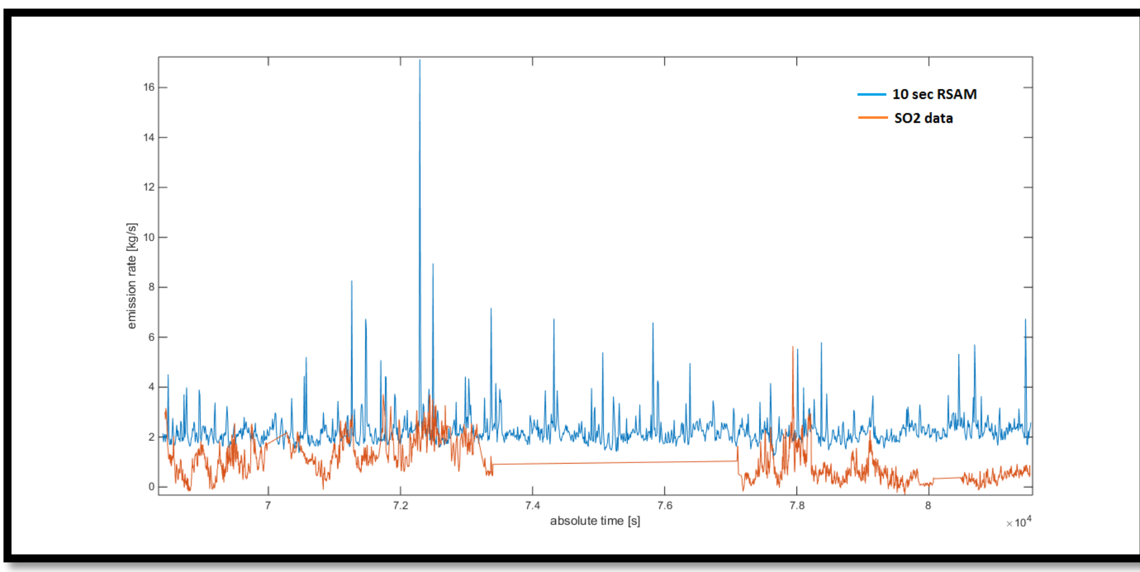

Figure 9- Plots of the 10sec RSAM and the SO_2 data of the 20th Jan 2015. The time is in absolute seconds of the day.

c) *Fieldwork Campaign in Guatemala*

The campaign started on the 9th of January and ended on the 25th of January 2015 after 2 weeks of sampling on the volcano. Weather conditions in January are in general the best of the entire year;

November through April constitutes the dry season in the Guatemala City region. These months are generally also the coldest and the windiest of the year as shown in Table 2 in the appendix.

During the field work the weather was always sunny, but the summit of Pacaya Volcano was rarely free from clouds, especially during the morning. The wind was usually present and strong, and was a hazard that impeded access to the summit for most of the campaign.

A total number of 440 measurements were made with the CO_2 accumulation chamber, principally from the northern side of the volcano. The inaccessibility of the southern side was mainly due to the hazard related to rock-falls and also to the elevated gradient of this area. Therefore, only a small number of measurements were made on the southern slopes of the volcano.

About 8000 images were obtained using an UV camera from the foot of Pacaya; the maximum distance from where the images were collected has been of 4.5 km from the volcanic plume. The clouds that covered the summit most of the time, allowed the use of the camera for portions of the day on the 19^{th}, 20^{th} and 21^{st} of January. The last day has been the noisiest, in fact were collected just 751 images versus the 5250 of the 19^{th} and the 1917 of the 20^{th}.

In addition to the diffuse degassing studies and UV camera images, seismological data were collected by a temporary network of seismic stations around the cone. We restrict our analysis to one station buried near the summit vent of the volcano, chosen because it is the closest point to the volcanic plume and also to the highest CO_2 fluxes.

5) Results

a) *Diffuse soil CO_2 flux*

The analysis of 440 flux measurements showed that the data can be divided into three different populations based on the cumulative frequency distribution. In fact, as shown in Fig. 10, two inflection points are observed in the cumulative frequency curve (red line). The first population, “background”, represents ~80% of the data, which range from 0.310 $g/m^2/day$ to 4 $g/m^2/day$. The second population, “mixed”, represents 8.5% of the data, which range from 4 $g/m^2/day$ to 20 $g/m^2/day$. The third population, “magmatic”, represents 11.5% of the data, which range from 20 $g/m^2/day$ to 15,489 $g/m^2/day$.

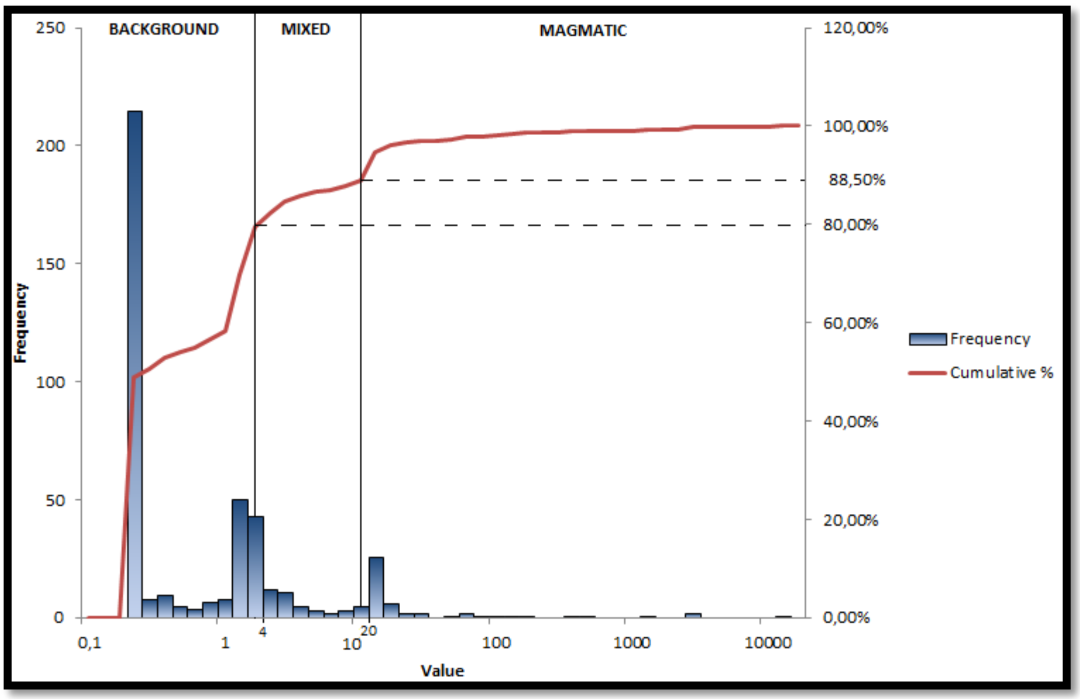

Figure 10- Cumulative distribution plot of the data. The black vertical lines represent break points at 3 and 20 g/m2/day.

The area on the north-eastern flank of the Pacaya volcano, with an area of 1.0 km², is characterized by fluxes which vary from a minimum value of 0.31 $g/m^2/day$ (LOD/√2) to a maximum value of 15,489 $g/m^2/day$. The mean value is equal to 17.04 $g/m^2/day$ with a standard deviation of 137.06 $g/m^2/day$. A total CO_2 output of 13.6 t/day was calculated using the ArcGis calculator multiplying the cells, or pixels, of 5 m^2 that compose the map (expressed in $g/m^2/day$). Furthermore, using the resultant values of the 100 sGs simulations - while retaining a 95% confidence interval - a minimum output of 9.6 t/day and a maximum output of 19.0 t/day, were simulated.

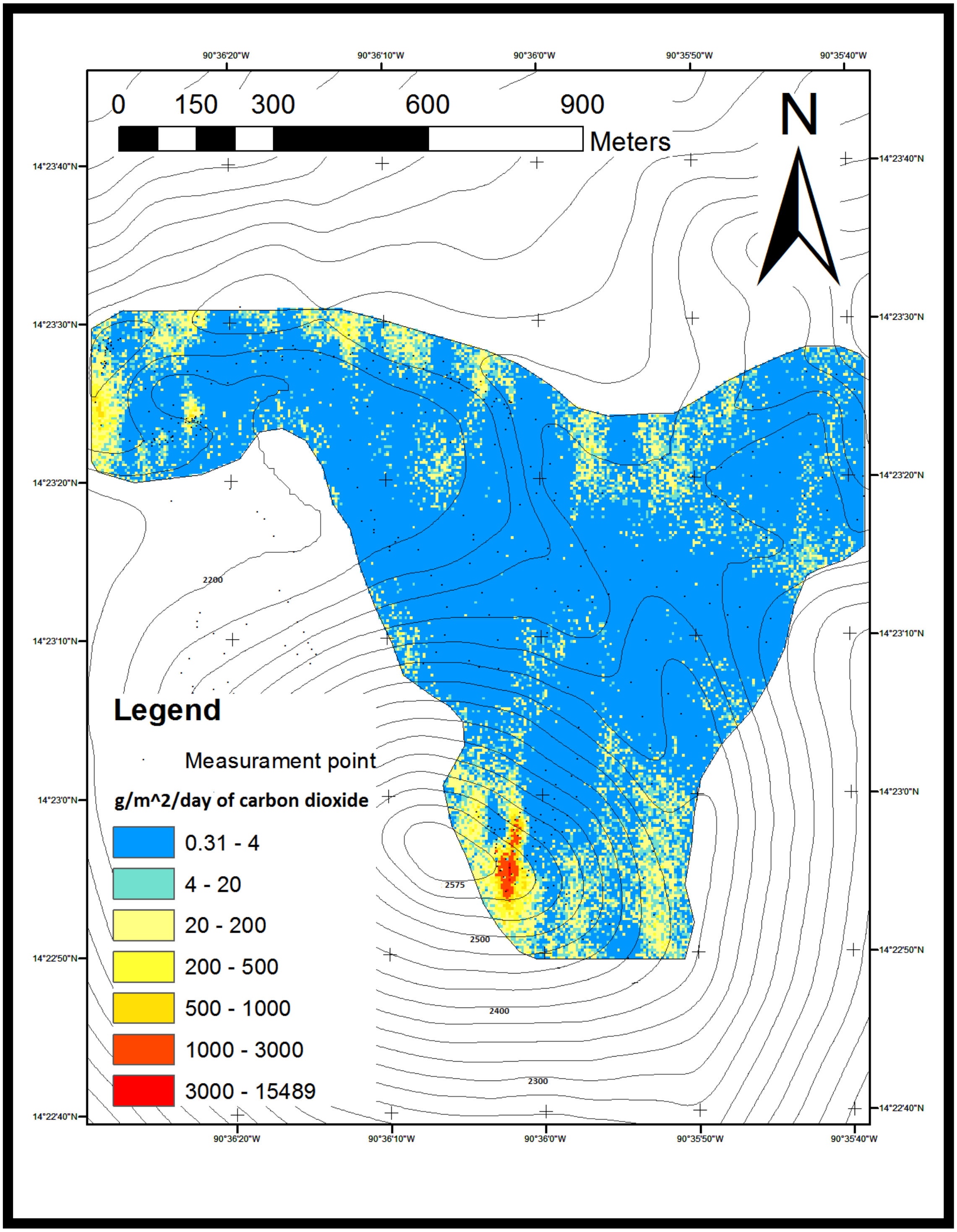

Figure 11- Flux map obtained from the sGs results. The population breaks has been kept as the first two colors. Warm colors correspond to high fluxes, vice versa the cold ones.

To construct this map, the GSLIB software requests the input of a semi-variogram model (blue line in Fig. 12). This model is built on the empirical semi-variogram (red dots in Fig. 12), that is obtained using the factors' values given by the geostatistical analyst tool of ArcGis 10.2 (e.g., lag size, number of lags, lag tolerance). The parameters input to obtain the model are: a nugget effect of 0.35, 400 lags, an a_hmax of 150 m, an a_hmin 60 m and no preferred directions for the diffuse degassing. The semi-variogram model shown in Fig. 12, which determines the spatial relationship between measurement locations and pixels of the map, is exponential and shows a spatial auto-correlation in the data (red dots) until a distance of about 400m. The data doesn't fit the semi-variogram well after a distance of 160m; in fact the model's variance reaches a value of 1 at about 200m, indicating that the modeled absence of spatial correlation between different measurement points has been set at distances bigger than 200m.

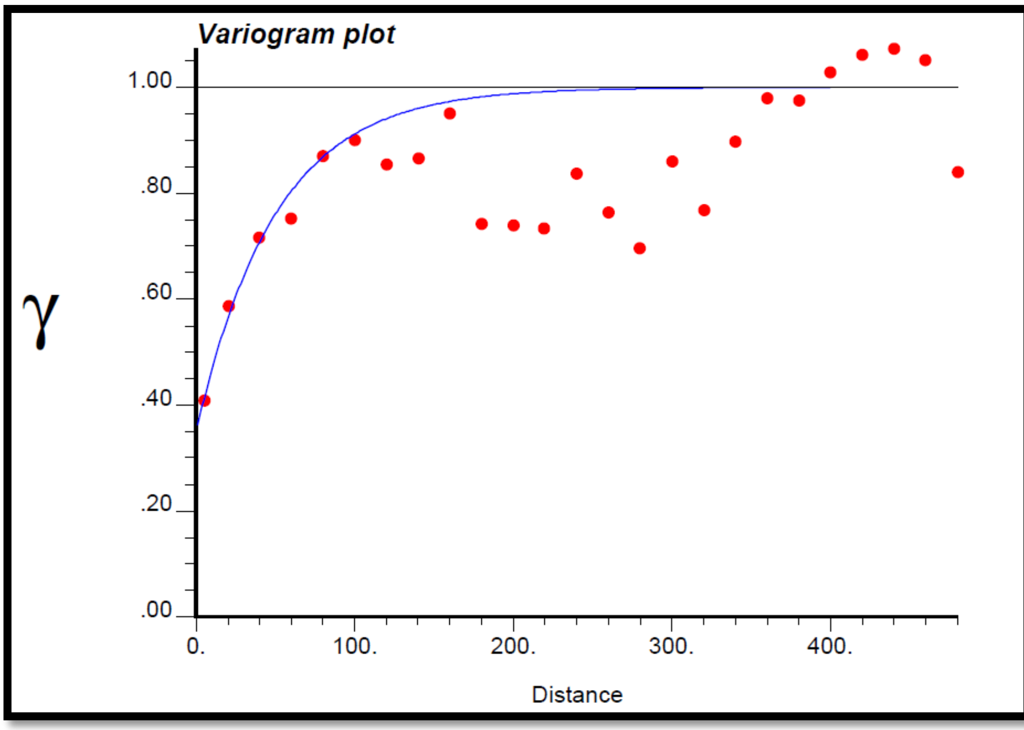

Figure 12- Semi-Variogram used for sGs of the CO2 flux. The Y-axis shows the variance value. The X-axis shows the distance in meters related to a certain value of variance. Red dots represent the data empirical semi-variogram. The blue line is the semi-variogram model fitted on the data.

The map shows a marked clustering of degassing structures. In fact, very high-fluxes are localized in the southern sector; whereas in the north-western sector some centers of diffuse degassing are noticeable and characterized by medium-high-fluxes of CO_2. Finally, the central area and the eastern corner present predominantly low fluxes related to the "background" and the "mixed" populations.

b) UV camera and seismic data

In order to reduce the error and the noise due to poor weather conditions (e.g. high wind speed and clouds), some UV images have been discarded; the resultant number of images is 2985 for the 19th

January, 1600 for the 20th January and 400 for the 21st. Recording times were ≈3.6, ≈1.25 and ≈0.9 hours, respectively. Only one ash-rich explosion was observed during the 3 days of sampling, it happened on the 20th at 20:05 UTC time and images that included that event were not used for emission calculations. So the passive degassing was almost always continuous but variable in magnitude. In Fig. 13 is shown the best day of acquisition with the UV camera. In fact during the 20th of January there were the best weather conditions and we needed to calibrate the camera only one time. The maximum obtained values for the emission rate are: 3.706 kg/s for the 19th, 1.148 kg/s for the 20th and 3.657 kg/s for the 21st.

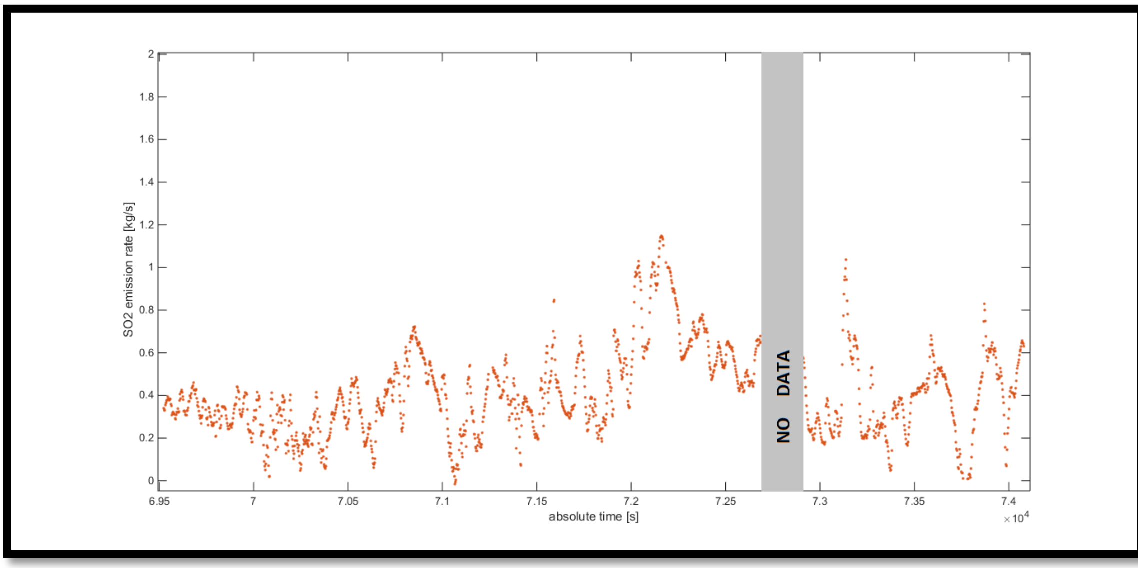

Figure 13- SO2 Emission rate plot of the 20th of January. The grey box in the picture represents the no data interval due to both a period of poor weather conditions and a calibration break.

The RSAM of all the three days were computed with a selected interval of time of 10 seconds (Fig. 14b) using the previously filtered seismic signals (Fig. 14a). Then from the interpolation of the SO_2 datasets we obtained vectors which have the same time spacing of the 10 seconds RSAM vectors, so they can be compared using the cross-correlation command.

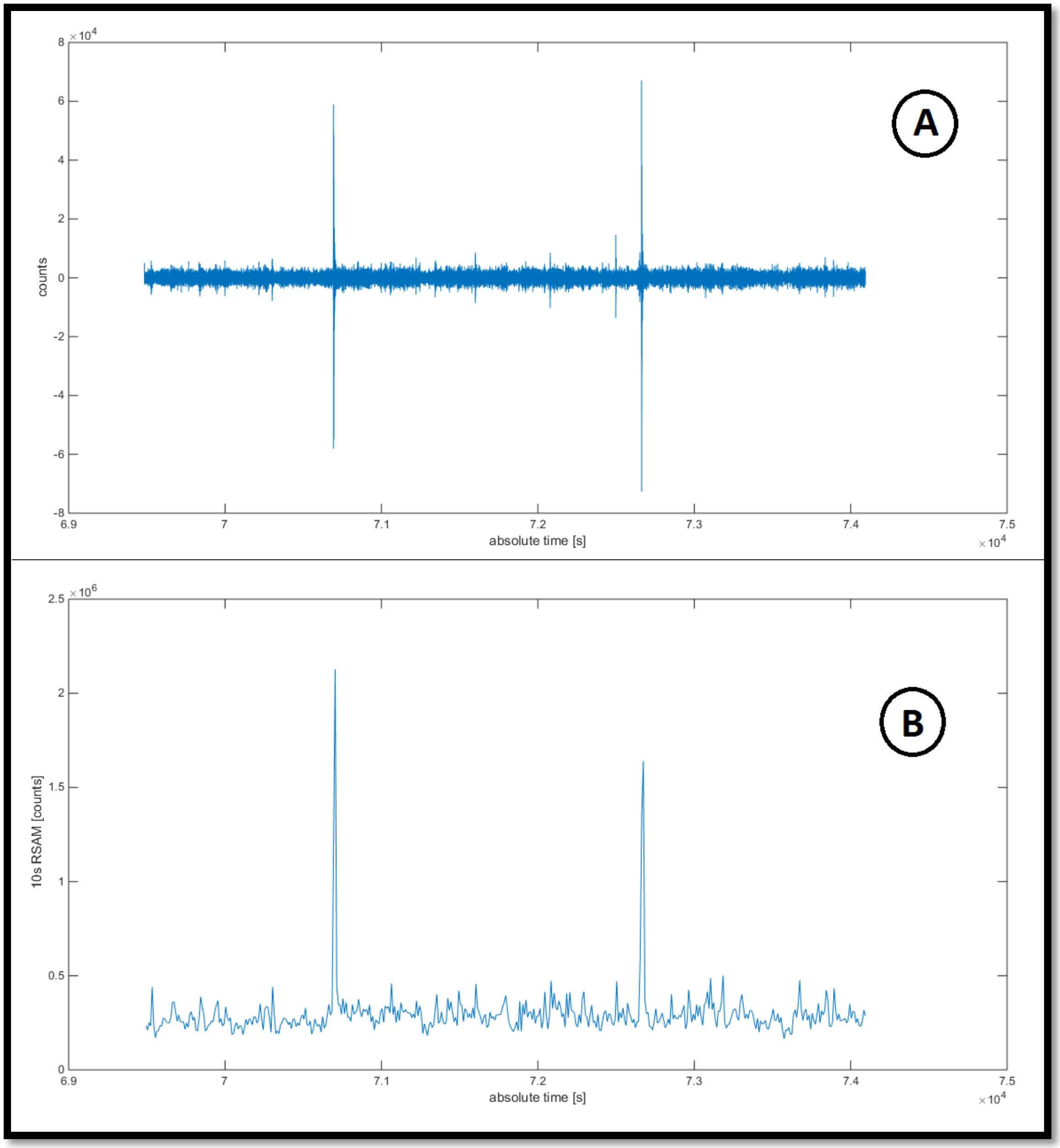

Figure 14- A) Selected interval of time (absolute seconds) of the seismic signal recorded on the 20th of January, the signal was filtered before plotting it. B) 10seconds RSAM of the filtered seismic signal.

From the cross-correlation process we obtained three plots, one per day, that show the lag in time between the two vectors at a certain value of time shifting (Fig. 15). The best cross-correlation value was obtained from the datasets of the 20th January; it has a value of 0.13 when the SO_2 is lagging 20 seconds behind the RSAM. The other days had different values of correlation and lags; in particular for the 19th we had the best correlation at 70 seconds of lag with a value of 0.08, whereas the data of the 21st shown a factor of 0.06 at 40 seconds of lag.

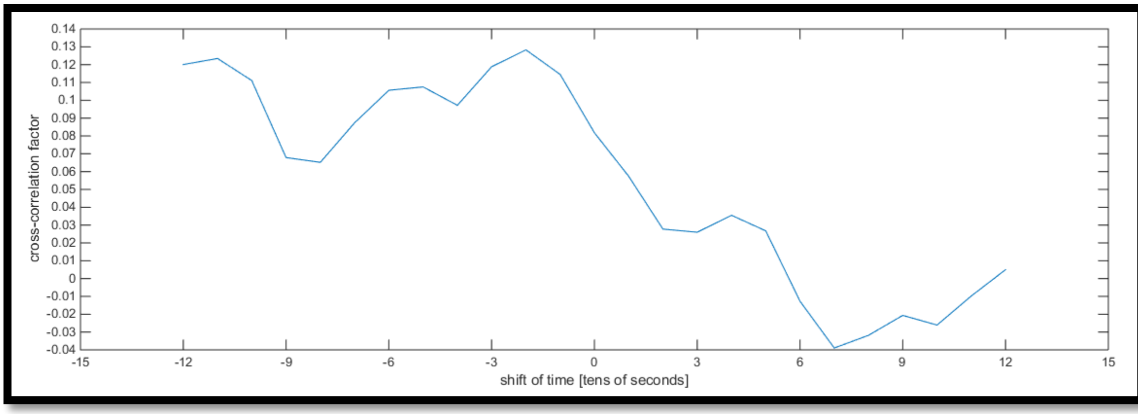

Figure 15- Cross correlation plot between the seismic data and the interpolated SO2 data.

Finally the 10 seconds RSAM have been plotted with the SO_2 emission rate plots to have a visual comparison of the datasets. In Fig. 16 is shown the plot of the day 20th of January 2015.

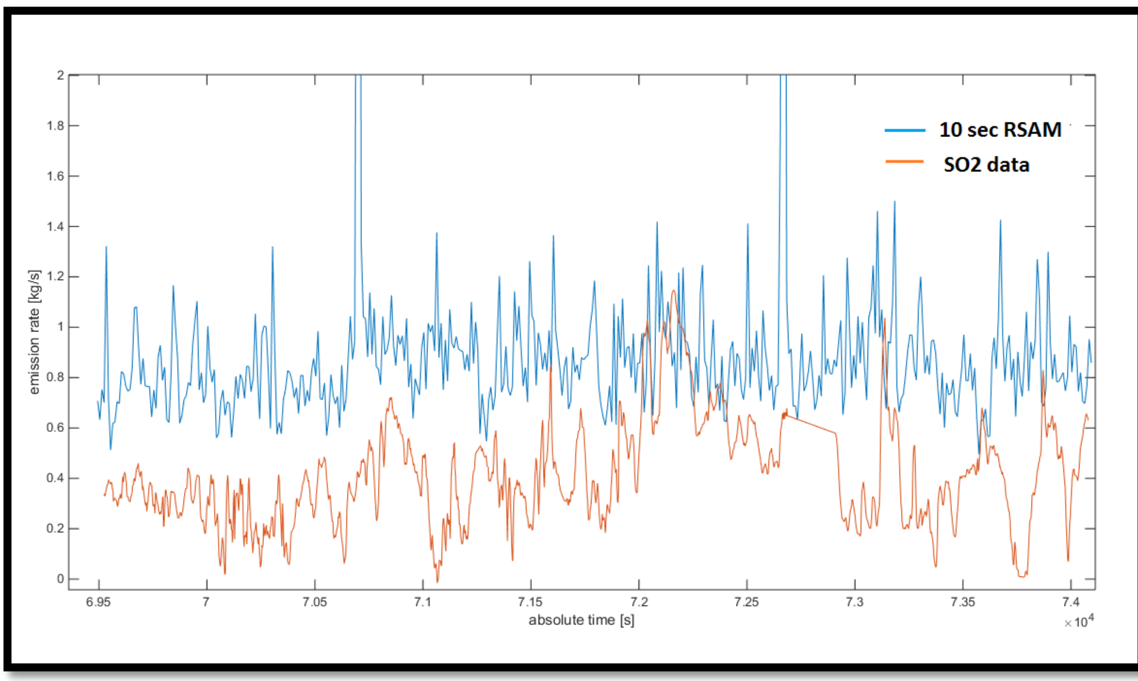

Figure 16- Example of similarity between SO2 emission rate (orange line) and low-frequencies 10 seconds RSAM (20th Jan).

6) Discussion

a) Diffuse soil CO_2 flux

The data collected in the investigated area of 1.0 km² on the north-eastern flank of Pacaya volcano permitted the calculation of total CO_2 output, which was 13.6 t/day. The first consideration to make about this result is that we have not discerned the "background" and the "mixed" flux populations from the "magmatic" one in our calculation process. In the entire sampled area the vegetation was poorly developed or lacking, the organic soil was absent and the ground was covered by tephra and new lava-flows. Furthermore, the absence of chemical data useful to distinguish between isotopes of carbon dioxide, which are fundamental to understand the origin of the flowing CO_2, didn't allow us to separate the populations (Chiodini et al., 2008; Rissmann et al., 2012; Harvey et al., 2015). Moreover the samples taken in proximity of the 2010 vents and outside the collapse rim don't show any peculiarity in terms of flux value; the 2010 vents' area is also characterized by developed vegetation but it doesn't induce any difference. This is probably because the dry season that causes a kind of dormancy in the vegetal apparatuses. Therefore, all of the measured CO_2 flux is considered magmatic in origin.

Our total CO_2 flux value is comparable with other studies conducted on active volcanoes. The typical flux is about 35-40 t/km^2/day as demonstrated by Chiodini et al. (1998), Frondini et al. (2004), Notsu et al. (2004), on Vulcano, Vesuvio and Iwojima volcanoes, respectively; although this is highly temporally variable and specific to each volcano. For example, Padròn et al. (2008) on Pululahua volcano found an output of only 9.8 t/km^2/day, whereas Salazar et al. (2001) obtained a final value of 2,800 t/day from an area of only 0.58 km^2 on Cerro Negro Volcano. Furthermore, Hernández et al. (2012) have demonstrated how the output of carbon dioxide of the same study area can be largely variable depending on the season and changes in weather conditions. Giammanco et al. (1998) and Meliàn et al. (2014) have also shown how the CO_2 output is variable through time also because the different level of activity of a volcanic system.

Obviously the location and the dimension of the surveys' area play a prime role in the quantification of the carbon dioxide efflux. We separated our investigated area into several discrete regions in order to remove the central "no flux" area (Fig. 11) and reduce the error related to the larger spacing between samples adopted in this portion of the map.

Figure 17 shows the maps of the two areas with "high-flux". The "Cerro Chino and Collapse Rim" (Fig. 17 section C) map covers an area of 0.180 km^2, whereas the "Summit Area" (Fig. 17 section B) covers 0.015km^2; these maps were created by 120 and 250 sGs simulations, respectively. The semi-variogram models are shown in Fig. 18 and show a spatial correlation up to 80 meters. The "Cerro Chino and Collapse Rim" (Fig. 17 section A) semi-variogram model is spherical; it has a nugget effect of 0.45, 150 lags, an a_hmax of 70 m, an a_hmin 25 m and no preferred orientation angles. The "Summit-area" (Fig. 17 section B) semi-variogram model is exponential; it has a nugget effect of 0.1, 120 lags, an a_hmax of 55 m, an a_hmin 15 m and no preferred orientation angles. Summing these two areas' outputs produced a total CO_2 output of 8 t/day with a 5th percentile of 4.7 t/day and a 95th percentile of 12.9 t/day from an area that is only 0.195 km^2. This value of 41 t/km^2/day is consistent with those that were found by Chiodini et al., Frondini et al. and Notsu et al.

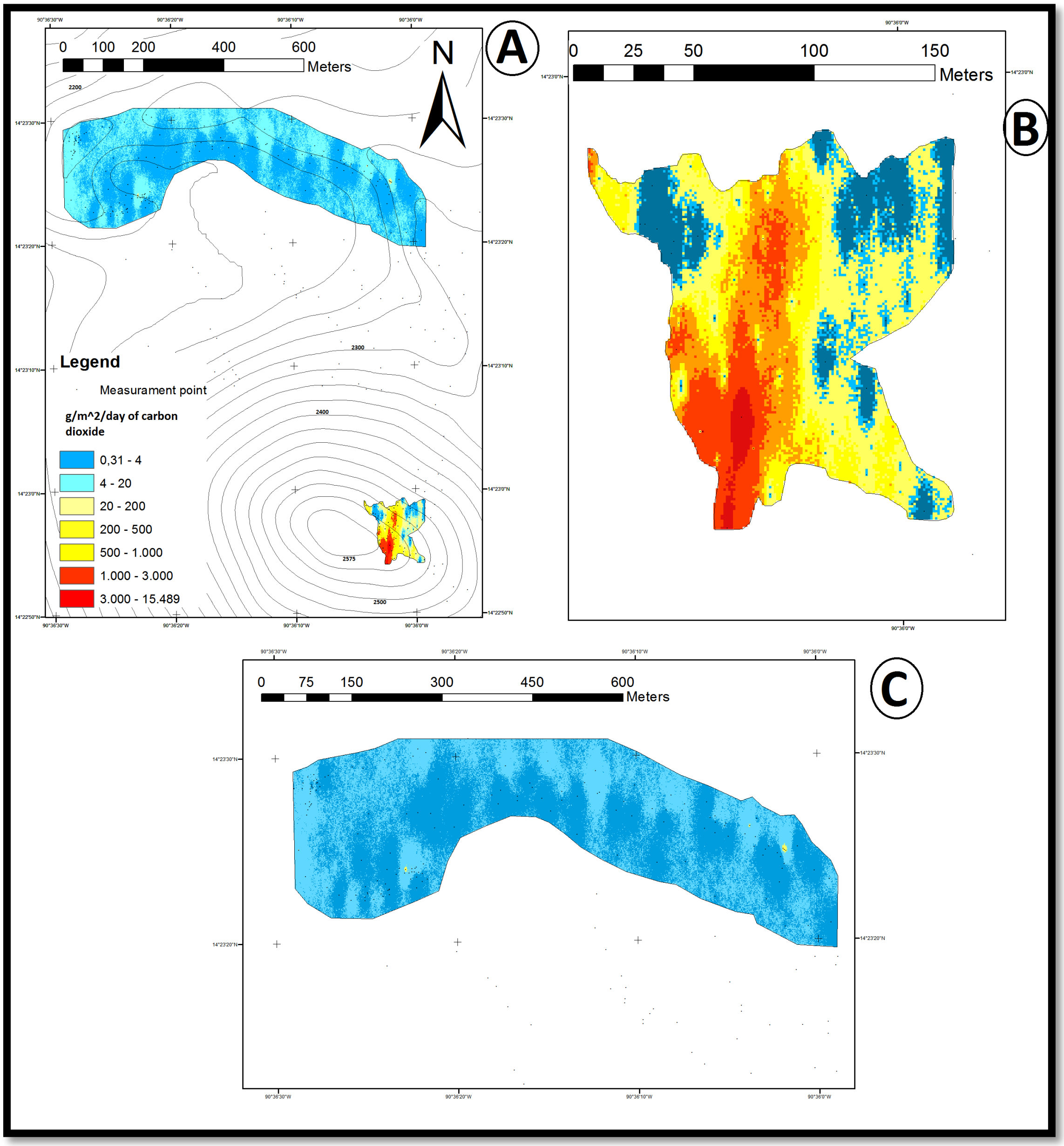

Figure 17- CO2 flux map of the "high-flux" areas. A) Overview of the areas. B) Zoom in of the summit area. C) Zoom in of the Cerro Chino-and-Collapse Rim area.

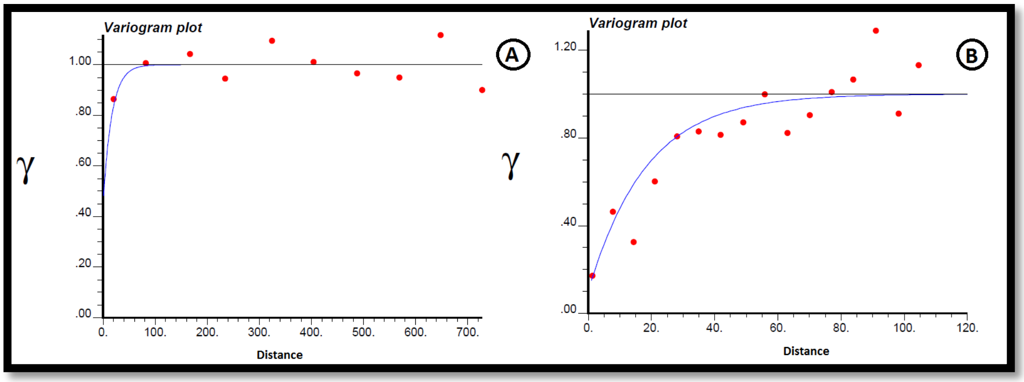

Figure 18- Variogram plots of the two "high flux" area. A) Cerro Chino and Collapse Rim area. B) Summit area.

Besides the estimation of the total CO_2 output, the carbon dioxide diffuse degassing investigations can also be used for geo-structural characterization of the studied areas. A large number of studies in the last two decades have demonstrated how the distribution of the highest flux in a map is localized along faults, a system of faults, eruptive fissures, fumaroles, or crater and collapse rims (Giammanco et al., 1998; Lewicki and Brantley, 2000; Chiodini et al. 2001; Cardellini et al., 2003; Frondini et al., 2004; Giammanco et al., 2006; Padrón et al., 2008; Ranaldi, 2008; Melián et al., 2014; Harvey and Harvey, 2015).

In our studied area, as is noticeable in Fig. 11 and in Fig. 17, we observed three different alignments of degassing spots and fissures. Overlaying the flux map with the most recent DEM on ArcGis we can highlight how the diffuse degassing follows the regional and local orientation of principal stresses and the geological structures (Fig 19). In this image it is evident that along the horse-shaped collapse rim and crater rim border of the Cerro Chino (Fig. 19), areas of the highest efflux of CO_2 are observed, reaching values greater than 500 g/m^2/day. We interpret these aligned degassing areas as being driven by the higher permeability due to the historic evolution of the volcanic complex; the horse-shaped rim is the continuation of the surface of contact between the materials of the "pre-phase three materials" and the "post-collapse materials". This surface of contact has been analyzed and described in detail by Schaefer et al. (2013).

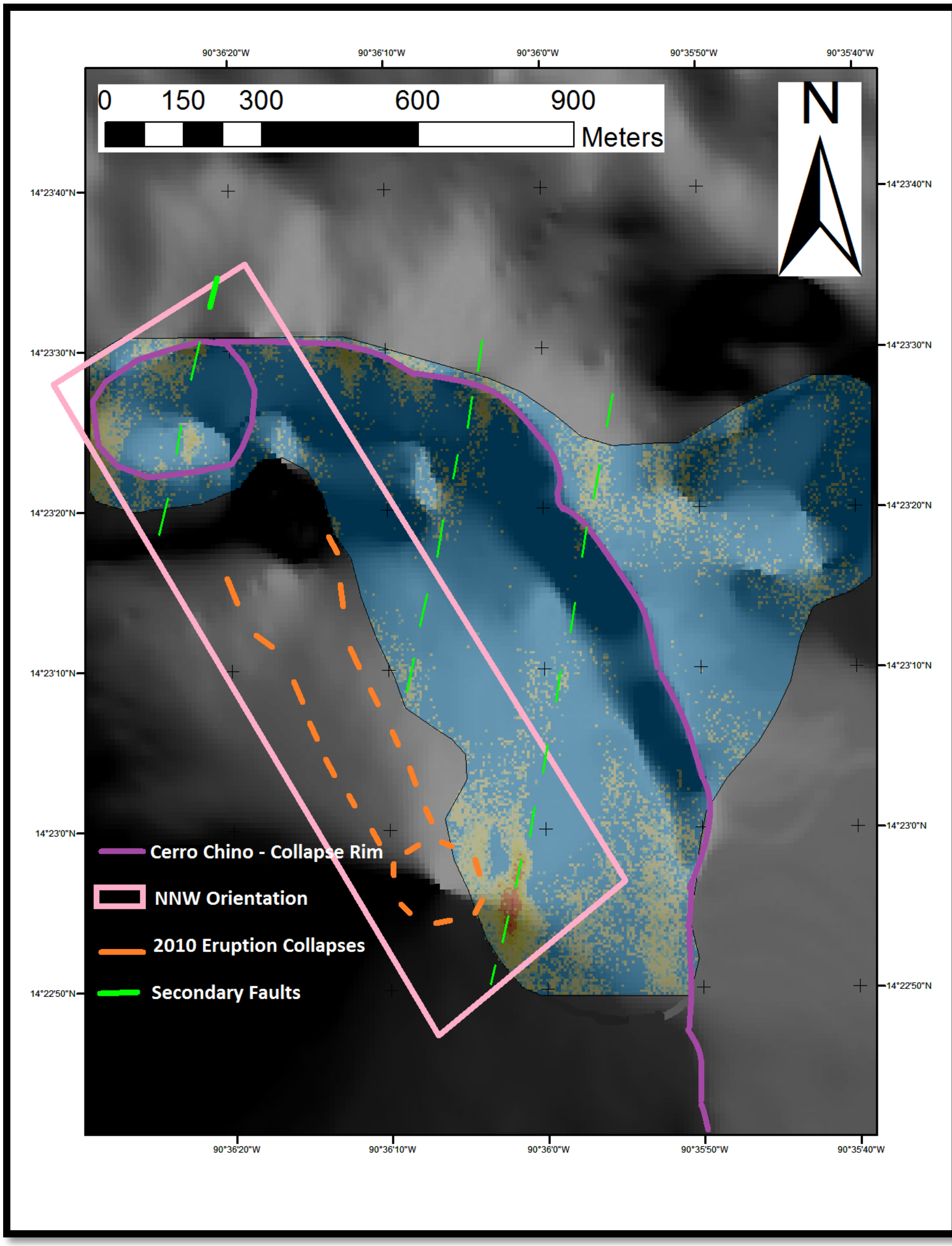

Figure 19- Digital image of the major features and orientation overlapped upon the DEM and the fluxes map.

In contrast, the degassing along the collapse-rim area of the Cerro Chino border is not interpreted to be related to the contact's surface, but is instead associated with a more complex interaction of structural features. First, the dip slope strata of the Cerro-Chino cone could concentrate the CO_2 diffuse degassing along the crater rim playing the role of a kind of upside down funnel. Second, they could be driven by the NNW magma ascent also described in Schaefer et al. (2013). The intrusion of the magma along the Jalpatagua fault zone (JFZ) creates a weakness zone that is more permeable and where the magma is closer to the surface; so this zone could be a preferable pathway for the degassing. This zone of weakness has been highlighted in Fig. 19 with a pink box showing the 2010 collapses (orange lines); important features that provide evidence of the enormous NNW collapse feature and orientation of the magma ascent. Aligned with the Cerro Chino's efflux points and the collapse is the summit area, where we recorded the highest fluxes. Furthermore, the field observations of this area highlight a highly fractured soil with numerous cracks and alignment of fumaroles with directions in between 300° N and 340° N. All these features can be linked with the 2010 vent locations as indicated by Rose et al. (2013) and Schaefer et al. (2013), which are well aligned with the NNW trend on the south-eastern flank of the volcano too.

Analyzing the Google Earth® imagery since the 2010 event we noticed that the opening of cracks, that probably caused the collapse through the NW flank, is not exclusive of the northern sector of the volcano. In fact, we mapped for the first time the opening of an eruptive fissure on the South-Eastern flank of the new cone; the opening has started after the 2010 eruption and continued during the 2014 eruption between February and March. Figure 20 shows the sequence of images captured on Google Earth, the orange ovals have been drawn to help visualize the features of interest during the three main steps: before the 2010 eruption, after the 2010 eruption and after the 2014 eruption. Figure 21 shows a comparison between the "after 2010 eruption" and the "after the 2014 eruption" digitized features.

In Fig. 19 a system of possible secondary faults has been highlighted (green lines); these hypothetical faults have no surface expressions, but are inferred based on the higher CO_2 flux values in coincident with the interceptions between these secondary faults and the principal geologic features of the volcanic complex (e.g. the NNW weakness zone and the collapse rim). In Fig. 17 it is evident how the degassing is "spotted" along the collapse rim; in order to highlight this in Fig. 22 we show the simple kriging map obtained with the GSLIB software using the same semi-variogram model used for the general map in Fig. 12 with a radius of 20 meters. Jolie et al. (2015) has also shown how the interceptions between faults are related to elevated values in the CO_2 diffuse degassing. Furthermore, it is clear in Fig. 17 section B that in the summit area there is an alignment of very-high flux values in the NNE direction. Rose et al. (2013) have also shown that on Pacaya there exists two different directions along which the vents are clustered; besides the NNW alignment of vents they have also recognized a NNE alignment that is the same direction found in this study for the secondary faults. Based on the preceding evidence we interpret the distribution of high gas emissions to be related to magma intruding in a direction NNW, which causes a field of stress that has a local maximum compression axis in the direction NNE; in preexisting weakness zones with direction parallel to the local $\sigma 1$, the compression could cause the opening of the cracks – a major permeable network that increases the CO_2 efflux in these zones.

Figure 20- Sequence of images of Pacaya volcano captured using Google Earth. The orange ovals represent the "interest area" (map souce: Google Earth. See the Appendix for documentation of permission to use this material)

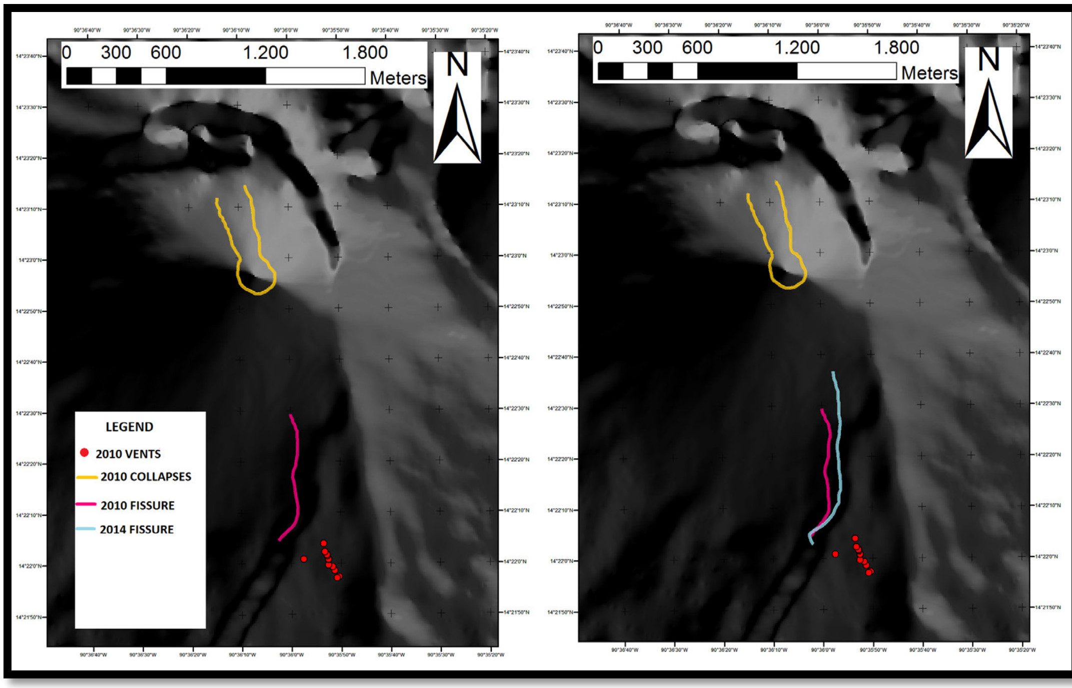

Figure 21- Comparison between feature originated in the 2010 eruption and features originated by the 2014 event.

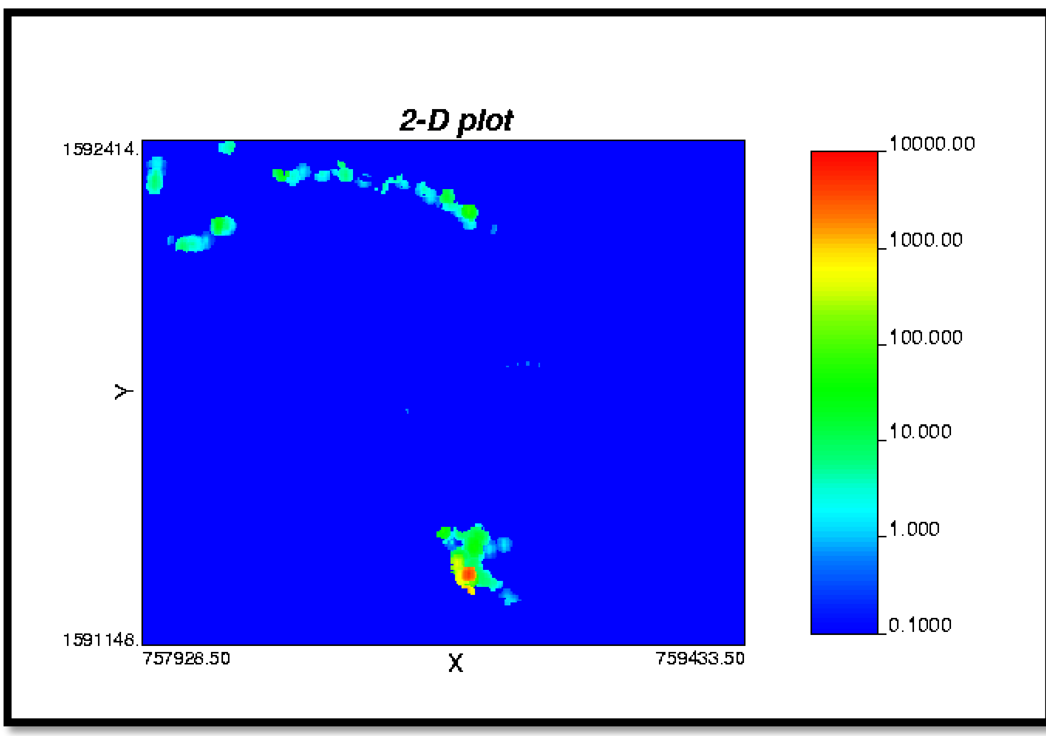

Figure 22- GSLIB Simple-Kriging map.

b) UV camera and seismic data

The fact that UV cameras can collect nearly an image every second makes of this instrument one of the most promising tools in the study of volcano degassing (Mori and Burton, 2006; Bluth et al., 2007; Dalton et al., 2009; Nadeau et al., 2011). In particular, the high sample rate of 1 sample every 1-3 seconds permitted to us to relate the UV camera data with the seismic dataset. For this comparison we used just the seismic signal that is in the long-period (LP) band between 0.5 and 5 Hz; this is because tremors and LP earthquakes are triggered by different processes that involve volcanic fluids. Numerous authors modeled these processes: Julian (1994 and 2000) affirmed that the fluid flow could be the responsible for very low-frequency events; Chouet proposed a model where he linked the seismic signal to conduit resonance (Chouet, 1992) and one in which he showed how the bubbles oscillation can effect the generation of low-frequency events (Chouet, 1996). Furthermore, working with Kumagai in 2000 (Kumagai and Chouet, 2000), he demonstrated how a crack filled by bubbly fluid can have enough impedance in respect the surrounding materials such that the crack can sustain resonance at certain frequencies for relatively long time. Ripepe and Gordeev (1999) linked the tremors and LP to bubble coalescence. Finally Métaxian et al. (1997) and Palma et al. (2008) show how the low-frequencies events can be related to the outgassing activity. The basic idea for linking outgassing with shallow LP seismicity is as follows: the larger is the quantity of gasses involved, the stronger the low-frequency seismic signal related to the same system (Fig. 23).

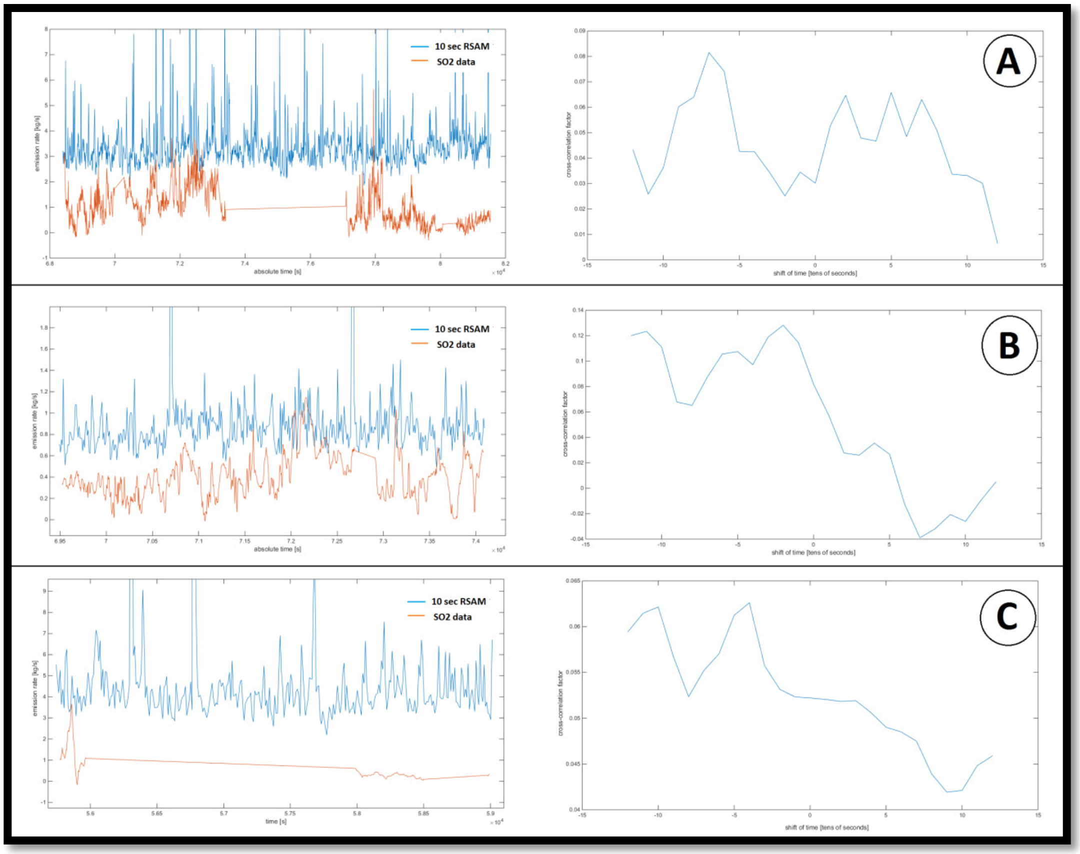

Figure 23- SO2 and 10s RSAM plot compared to each cross correlation plot. A) 19th Jan 2015 plots. B) 20th Jan 2015 plots. C) 21th Jan 2015 plots.

Following this principle we compared the two dataset without giving too much importance to the value of mass of gasses emitted during the day, but caring much more about the trend of the degassing. We chose to use a RSAM of 10 seconds because it is the interval that produced the best cross correlation values. The cross correlation values are not very high compared with those in the studies of Kazahaya et al. (2011) and Nadeau et al. (2011), most likely because of suboptimal weather conditions for much of the field campaign. Nonetheless, the datasets show a correlation that permits to us to suggest that the trend of the SO_2 degassing is linked to the seismic signal (Fig. 23). This is evident if you in the clear correspondence of the troughs of the two datasets. With a bigger database, the correlation factor would likely be greater, but having a clear view of the Pacaya's plume and at the same time a clear sky for the background is really difficult.

The different lag values that we have found during the three days could be related to changes in the conduit, for example a different depth of the magma's surface, but also in this case the uncertainty, especially for the 19th and the 21st is too big to permit any comparison between different days.

Interestingly, although the outgassing characteristics were apparently different in January 2015 than they were in 2008 when Dalton et al. (2010) got their data, we calculate a comparable output of SO_2 So while it was easier to distinguish individual explosions in 2008 due, presumeabley to a much shallower magma free surface, it seems that the SO_2 degassing from Pacaya continues to driven by small bubble-burst events.

7) Conclusions

This study was based on field data collected on Pacaya volcano (Guatemala) in January 2015. The use of advanced techniques and software for the investigation of the volcanic degassing permitted the collection of a large amount of new data, which are important, not only for this work, but also for future studies that will be carried out on this volcano..

The portable diffuse flux-meter made by West System S.r.l. proved to be a reliable instrument that permits a detailed characterization of a large area. Diffuse efflux measurements of volcanic CO_2 were used to calculate total outputs of: 13.6 t/km^2/day from the northern side and 41 t/km^2/day from the only other area where there are degassing features. These estimates are slightly lower than, but consistent with, those previously reported in the literature for other volcanoes.

Besides the estimation of the total CO_2 output, this study has demonstrated that the accumulation chamber method is complementary to structural studies. In fact, we show how the diffuse efflux measurements on Pacaya highlighted not only the NNW oriented faults and fractures, but also the structural features such as the collapse rim. Furthermore, this technique has revealed a NNE orientation of structural features, which are not evident on the surface. This orientation is similar to the trend of alignment of vent clusters recently summarized by Rose et al. (2013), and could be related to the interaction between local and regional stresses with preexisting structures, or to the intersection of faults. However the combination of all these factors is, most likely the cause of the NNE alignment of fluxes.

By combining the high-resolution SO_2 emission rates obtained with the UV-camera and the 10 seconds RSAM we identified similar time scales for plume degassing and low-frequencies seismic events. In particular we observed a SO_2 signal that lags 20-40 seconds behind the seismic one with a peak of emission rate of 3.706 kg/s registered on the 19th January 2015.

Even if during our field campaign we didn't recorded any noticeable explosive event, our field observations and results support the thesis of a Strombolian bubble-burst activity proposed by Dalton et al. in the 2010; this activity is less noticeable in our data because a deeper source of the events (the lava free surface must be deep in the conduit).

In light of what we showed and what we observed in the field, we suggest that Pacaya has an open conduit with a small lava lake (Fig. 24) that is fed by a very shallow intruding magma body elongated in the NNW direction. Magma ascent and intrusions are opening new cracks all over the volcano, which will probably create instabilities - especially in the new dome.

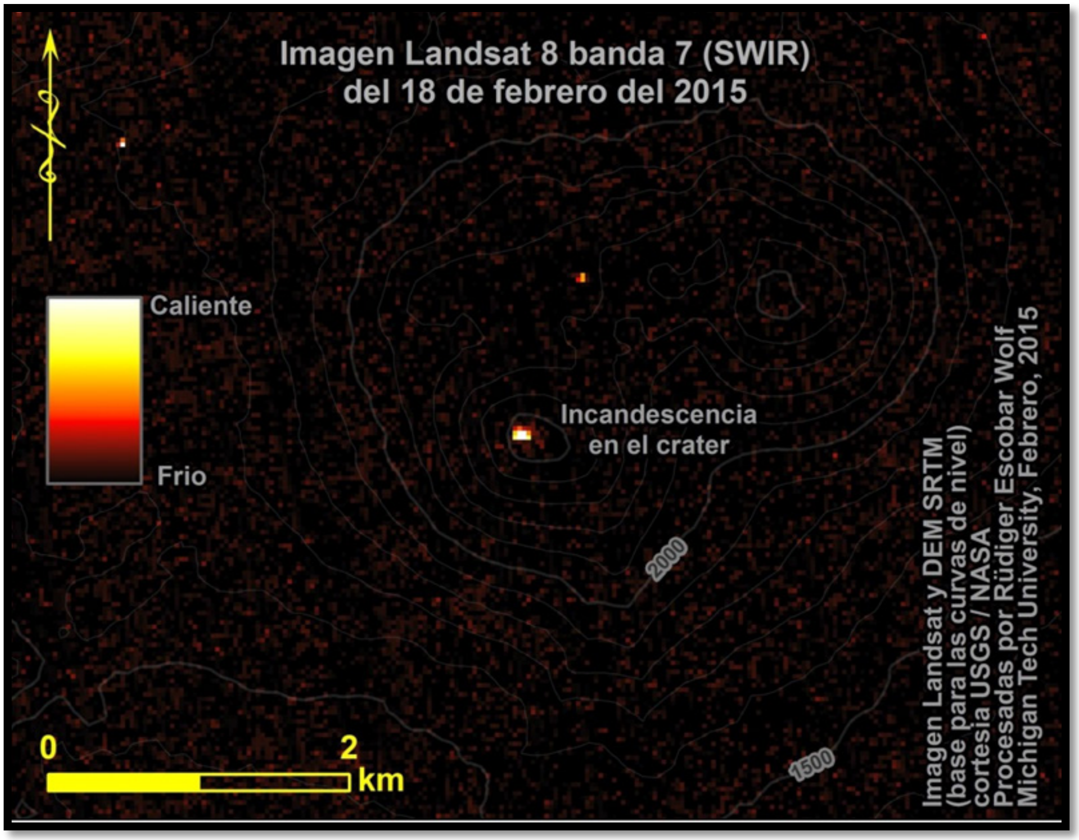

Figure 24 - Landsat 8 band #7 image of the Pacaya's summit of the 18 February 2015. In the center of the image (active crater's position) is evident an incandescence (white and yellow pixels) that proves the presence of a really high temperature source nearby the surface (R. Escobar-Wolf, personal communication, July 2015. See the Appendix for documentation of permission to use this material).

8) Recommendations for future research

Below we summarize some ideas for further investigations about the outgassing of Pacaya. In fact, our observations – in addition to improving our immediate knowledge of the structural magmatic, and gas emissions - reveal future avenues for studies that will expand the utility of this work. In this chapter we made a list of questions that need a solution and make some suggestions for how to answer them.

Variable fluxes

During our field work and data processing we observed ten flux curves that are not linear as the "perfect" curve described in the West System's handbook. They show a trend that is similar to the curves that present air contamination during the sampling procedure (Fig. 25). All these samples were taken near the summit, where the immature soil and rock are highly fractured and covered by fresh tephra, directly on fumaroles. The outgassing of these vents was following the outgassing through the volcano summit with only a short lag of time. Also the CO_2 curves followed the trend of the fumaroles and they were going up and down just after respectively growths and the drops of the principal summit plume. We interpret the non-linear trends in our curves as not being due to air contamination, but rather the gas pulses observed at the summit. We attempted to test this hypothesis by plotting the CO_2 "variable" fluxes with the 5 second RSAM of the seismic signal using a code written for Matlab. In order to have a better visualization of the data we normalized and de-trended the CO_2 curves (Fig. 26). The biggest problem that we noticed in this process was the uncertainty linked to the time that is necessary to save the data using the West Systems hand-held Trimble computer after the measurement has been stopped. In fact, the hand-held computer records the samples imprinting the saving time instead of the time related to the end of the measurements. The time between the end of a measurement and that for saving is artificially shifted for the CO_2 curve, so it's possible to have the CO_2 signal precede the seismic signal. Although this method of 'correcting' for the time lag between measurement and recording induces some uncertainty in our interpretations, there appears to be a correlation between seismic and diffuse CO_2 degassing signals. Further research on these observations could open a new field of studies in the possible uses of the accumulation chamber and also it will be out of this a new tool for the Early warning system.

Solutions: Install a **permanent CO_2 accumulation chamber station** upon the cracks nearby the summit or collect **more samples with a standard procedure,** in order to eliminate the lag of time between the end of the sampling and the saving, from the same area.

UV-camera data vs. accumulation chamber data

The comparison between these two instruments' datasets could be interesting to see if there is a relationship between the CO_2 efflux from the soil and the SO_2 outgassing from the volcanic plume. Furthermore the lag of time between the UV-camera and the accumulation chamber data could give back information about the permeability of the soil and so its grade of fracturing.

Solutions: Install a **permanent CO_2 accumulation chamber station** upon the cracks nearby the summit or **work simultaneously in two separate teams** one with the UV-cam and the other with the accumulation chamber on the summit area and a standard procedure.

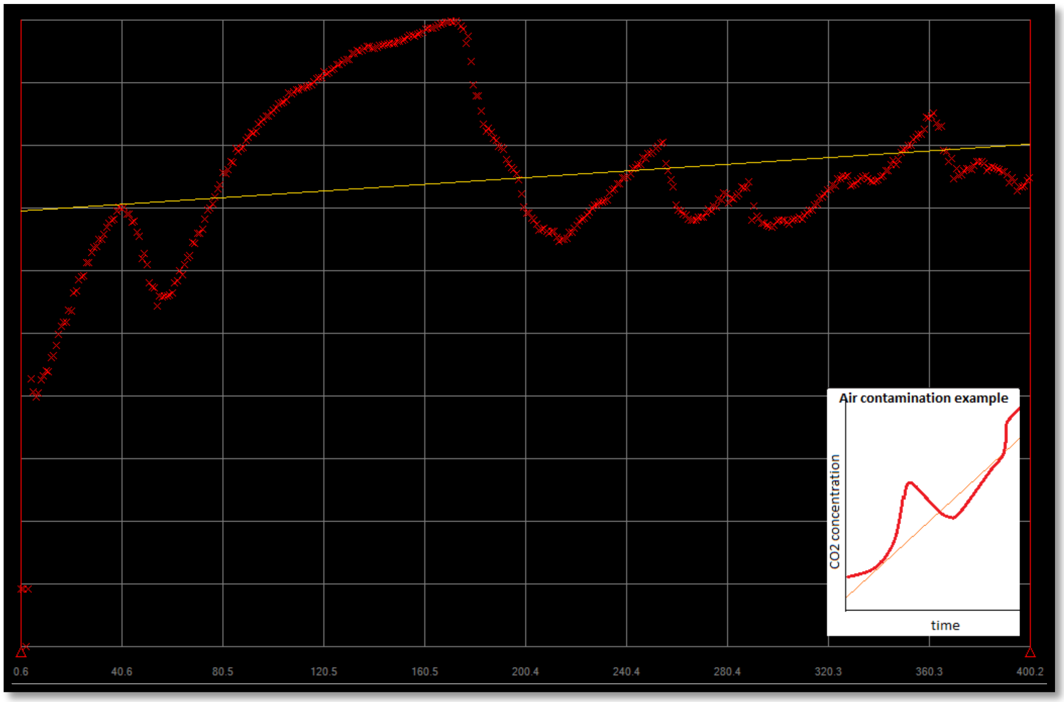

Figure 25- Example of variable flux (sample #300). In the white box is reported an example of a curve with air contamination.

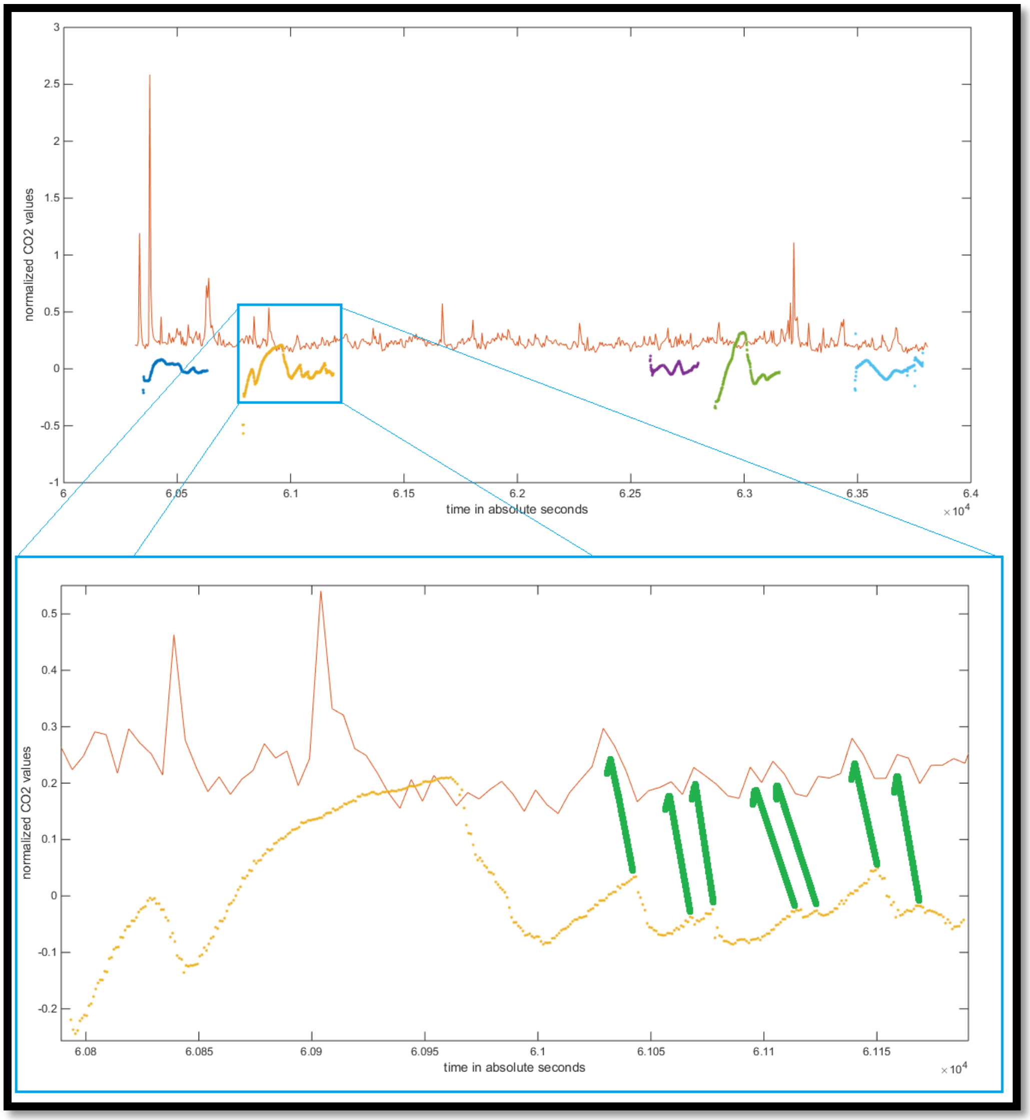

Figure 26- Comparison between seismic and CO2 samples of the 19th January 2015. The bottom part of the picture shows the zoom on the sample #300 showed in the previous figure.

Better CO_2 efflux map

Making additional measurements of diffuse CO_2 flux with the smaller accumulation chamber could provide a more detailed map with less points where the flux is smaller than the LOD. Furthermore, more samples on the south-eastern side could also provide some interesting information about the opening crack and the location of future vents. However, we are aware that measurements will be limited to the areas that are away from the rockfalls and if work is to be done near the summit fireproof and protective equipment will need to be worn.

Solutions: make a **grid with a smaller spacing** between sample points. **Use a chamber type A** that has a smaller LOD. **Try to expand the examined area**.

Structural map

A detailed geo-structural map can confirm our thesis about the secondary faults that we have found with the accumulation chamber, and provides more details that will improve the knowledge of the volcano.
Solution: **field campaign or campaigns of structural survey.**

More UV-cam data associated with both infrasound and seismic data
Collecting more data from the same period of time with more samples per day and relate them with both the infrasound and seismic data will be important to confirm and support this study's results.
Solutions: **a dedicated team for the UV-camera** sampling and a longer period of time on Pacaya.

Accurate SO_2 fraction in the plume
Having an accurate estimation of the SO2 fraction in the plume is important to reduce the error linked to the measurements with the UV-camera that is caused by other gasses in the plume.
Solution: analysis with the **Fourier Transform Infrared Spectroscopy (FTIR).**

Origin of the CO_2 and SO_2
Knowing the original composition of the magmatic fluid could reveal how much CO_2 and SO_2 are dissolved in the magma underneath the volcano and at what deep they start to escape from the magma. Regarding the CO_2 it's important to distinguish between the biogenic and the magmatic source using the carbon isotopes.
Solution: **Measurement of molten inclusions** and **Chemical analysis of carbon isotopes**.

Seasonal variation
Understand how the CO_2 total flux varies seasonally could be interesting to have an idea on how the weather, especially the rainfalls, influences the efflux.
Solution: **a field campaign every 4-6 months** (at least one for the dry season and one for the wet season).

CO_2 captured by the groundwater
A large fraction of the CO2 degassed from the magma could be trapped and washed away by the groundwater, knowing this fraction is fundamental to understand the total output of Pacaya.
Solution: **groundwater analysis.**

9) Acknowledgements

First of all I would like to thank my advisers Gregory P. Waite and Chad Deering for the amazing opportunity to go in Guatemala on Pacaya Volcano. Their fundamental guidance, suggestions and ideas made me work hard but now I'm very proud of this work. Finally I would like to thank them for their personal kindness and for their time spent with me.

Many thanks to the University of Milano-Bicocca and to Alessandro Tibaldi for founding and supporting the INVOGE program for many years.

Many thanks to the Fede's Group (Federica Lanza, Chet Hopp, Maximilian Guettinger, Kyle Brill and Hans Lechner) for the logistic support and to Nicola Mari for his help with the UV-cam studies.

A special thanks to Peipei Lin and Aurelia Liegler for the time spent together the lab, for their guidance, feedback and discussions - I would be lost without you!

Furthermore I would like to thank Rudiger Escobar-Wolf, Cindy Werner, Theodore Bornhorst and Davide Continanza for their technical support, suggestions and feedback.

Finally I would like to thank all my friends for motivating and distracting me in the everyday research life; a special thank you to my "American" friends and office mates for their corrections, you guys taught me to speak English!

Last but not least, I thank my family for making the Invoge opportunity possible and obviously for their infinite love; I would like to thank Jordan Lubbers and Riccardo Tortini too because they have been a kind of family in my Houghton experience.

10) References

Bardintzeff, J. M., & Deniel, C. (1992). Magmatic evolution of Pacaya and Cerro Chiquito volcanological complex, Guatemala. Bulletin of volcanology, 54(4), 267-283.

Bluth, G., Shannon, J.,Watson, I., Prata, A., Realmuto, V., 2007. Development of an ultra-violet digital camera for volcanic SO2 imaging. J. Volcanol. Geotherm. Res. 161, 47–56.

Burkhart B, Self S (1985). Extension and rotation of crustal blocks in northern Central America and effect on the volcanic arc. Geology 13:22–26.

Burton, M. R., Salerno, G. G., D'Auria, L., Caltabiano, T., Murè, F., & Maugeri, R. (2015). SO 2 flux monitoring at Stromboli with the new permanent INGV SO 2 camera system: A comparison with the FLAME network and seismological data. Journal of Volcanology and Geothermal Research.

Carr M (1976). Underthrusting and Quaternary faulting in northern Central America. Geol Soc Am Bull 87:825–829.

Cardellini, C., Chiodini, G., Frondini, F., 2003a. Application of stochastic simulation to Co2 flux from soil: Mapping and quantification of gas release. J. Geophys. Res. 108, 1–13. doi:10.1029/2002JB002165.

Chiodini, G., Cioni, R., Guidi, M., Raco, B., Marini, L. (1998). Soil CO2 flux measurements in volcanic and geothermal areas. Appl. Geochemistry 13, 543–552. doi:10.1016/S0883-2927(97)00076-0.

Chiodini, G., Frondini, F., Cardellini, C., Granieri, D., Marini, L., Ventura, G. (2001). CO2 degassing and energy release at Solfatara volcano, Campi Flegrei, Italy. J. Geophys. Res. 106, 16,213–16,221.

Chiodini, G., Caliro, S., Cardellini, C., Avino, R., Granieri, D., & Schmidt, A. (2008). Carbon isotopic composition of soil CO 2 efflux, a powerful method to discriminate different sources feeding soil CO 2 degassing in volcanic-hydrothermal areas. Earth and Planetary Science Letters, 274(3), 372-379.

Chouet, B. (1992), A seismic model for the source of long-period events and harmonic tremor, in Volcanic Seismology, edited by P. Gasparini, R. Scarpa, and K. Aki, pp. 133–156, Springer, New York.

Chouet, B. A. (1996), New methods and future trends in seismological volcano monitoring, in Monitoring and Mitigation of Volcano Hazards, edited by R. Scarpa and R. Tilling, pp. 23–98, Springer, Berlin.

Conway, F.M., Diehl, J.F., and Matias, O. (1992). Paleomagnetic constraints on eruption patterns at the Pacaya composite volcano, Guatemala: Bulletin of Volcanology, v. 55, no. 1–2, p. 25–32, doi:10.1007/BF00301117.

Croghan, C.W., Egeghy, P.P. (2003). Methods of Dealing with Values Below the Limit of Detection using SAS. SAS Institute Inc, 5pp.

Dalton, M. P., I. M. Watson, P. A. Nadeau, C. Werner, W. Morrow, and J. M. Shannon (2009), Assessment of the UV camera sulfur dioxide retrieval for point source plumes, J. Volcanol. Geotherm. Res., 188, 358–366 doi:10.1016/j.jvolgeores.2009.09.013

Dalton, M.P., Waite, G.P., Watson, I.M. and Nadeau, P.A., 2010. Multiparameter quantification of gas release during weak Strombolian eruptions at Pacaya Volcano, Guatemala. Geophysical Research Letters, 37.

Deutsch, C.V., Journel, A.G., 1998. GSLIB: Geostatistical software library and user's guide. Oxford University Press, 361 pp.

Eggers, A. A. (1971). The geology and petrology of the Amatitlán Quadrangle, Guatemala. PhD Dissertation, Dartmouth College.

Eggers A (1983). Temporal gravity and elevation changes at Pacaya volcano, Guatemala. J Volcanol Geotherm Res 19:223–237

Endo, E. T., and T. Murray (1991), Real-Time Seismic Amplitude Measurement (RSAM): A volcano monitoring and prediction tool, Bull. Volcanol., 53, 533–545, doi:10.1007/BF00298154

Franco A, Lasserre C, Lyon-Caen H, Kostoglodov V, Molina E, Guzman-Speziale M, Monterroso D, Robles V, Figueroa C, Amaya W, Barrier E, Chiquin L, Moran S, Flores O, Romero J, Santiago JA, Manea M, Manea VC (2012). Fault kinematics in northern Central America and coupling along the subduction interface of the Cocos Plate, from GPS data in Chiapas (Mexico), Guatemala and El Salvador: kinematics in northern Central America. Geophys J Int 189(3):1223–1236

Frondini, F., Chiodini, G., Caliro, S., Cardellini, C., Granieri, D., & Ventura, G. (2004). Diffuse CO2 degassing at Vesuvio, Italy. Bulletin of volcanology, 66(7), 642-651.

Frondini, F., Caliro, S., Cardellini, C., Chiodini, G., Morgantini, N., Parello, F. (2008). Carbon dioxide degassing from Tuscany and Northern Latium (Italy). Glob. Planet. Change 61, 89–102. doi:10.1016/j.gloplacha.2007.08.009

Giammanco S, Gurrieri S, Valenza M (1997) Soil CO2 degassing along tectonic structures of Mount Etna (Sicily): the Pernicana fault. Appl Geochem 12 :429–436

Giammanco, S., Gurrieri, S., & Valenza, M. (1998). Anomalous soil CO2 degassing in relation to faults and eruptive fissures on Mount Etna (Sicily, Italy). Bulletin of Volcanology, 60(4), 252-259.

Giammanco, S., Gurrieri, S., & Valenza, M. (2006). Fault-controlled soil CO2 degassing and shallow magma bodies: summit and lower east rift of Kilauea volcano (Hawaii), 1997. pure and applied geophysics, 163(4), 853-867.

Guzman-Speziale M (2001). Active seismic deformation in the grabens of northern Central America and its relationship to the relative motion of the North America-Caribbean plate boundary. Tectonophysics 337:39–51.

Harvey, M. C., & Harvey, C. C. (2015). Soil CO2 flux surveys: A review of the techniques in geothermal exploration. In Proceedings World Geothermal Congress 2015, Melbourne, Australia, 19-25 April 2015 (paper accepted).

Hernández, P. A., N. M. Pérez, T. Fridriksson, J. Egbert, E. Ilyinskaya, A. Thárhallsson, G. Ívarsson, G. Gíslason, I. Gunnarsson, and B. Jónsson (2012), Diffuse volcanic degassing and thermal energy release from Hengill volcanic system, Iceland, Bulletin of volcanology, 74, 2435-2448.

Hinkle, M.E. (1994). Environmental conditions affecting concentrations of He, CO2, O2 and N2 in soil gases. Appl. Geochemistry 9, 53–63. doi:10.1016/0883-2927(94)90052-3.

IGN, Bonis S (1993). Mapa geologico de Guatemala escala 1:250,000. Hoja ND 15-8-G, “Guatemala”. First edition (map), Guamatala

IGN, Eggers A (1969). Mapa geologico de Guatemala escala 1:50,000. Hoja 2059 II G, “Amatitlan”. First edition (map), Guatemala

Kantzas, E. P., McGonigle, A. J. S., Tamburello, G., Aiuppa, A., & Bryant, R. G. (2010). Protocols for UV camera volcanic SO 2 measurements. Journal of Volcanology and Geothermal Research, 194(1), 55-60.

Kazahaya, R., Mori, T., Takeo, M., Ohminato, T., Urabe, T. and Maeda, Y., 2011. Relation between single very-long-period pulses and volcanic gas emissions at Mt. Asama, Japan. Geophysical Research Letters, 38

Kitamura S, Matías Gómez RO (1995). Tephra stratigraphic approach to the eruptive history of Pacaya volcano, Guatemala. Science Reports—Tohoku University, Seventh Series. Geography 45(1):1–41.

Kumagai, H., and B. A. Chouet (2000), Acoustic properties of a crack containing magmatic or hydrothermal fluids, J. Geophys. Res., 105, 25,493–25,512, doi:10.1029/2000JB900273.

Lewicki, J. L., & Brantley, S. L. (2000). CO2 degassing along the San Andreas fault, Parkfield, California. Geophys. Res. Lett, 27(1), 5-8.

Lyon-Caen H, Barrier E, Lasserre C, Franco A, Arzu I, Chiquin L, Chiquin M, Duquesnoy T, Flores O, Galicia O, Luna J, Molina E, Porras O, Requena J, Robles V, Romero J, Wolf R

(2006). Kinematics of the North America-Caribbean-Cocos plates in Central America from new GPS measurements across the Polochic-Motagua fault system. Geophys Res Lett 33:1–5.

Mann, P., Rogers, R., and Gahagan, L.M. (2007). Overview of plate tectonic history and its unresolved tectonic problems, *in* Bundschuh, J., and Alvarado, G., eds., Central America: Geology, Resources and Hazards (vol. 1): London, Taylor & Francis, p. 201–237.

Manual of the ICAO Standard Atmosphere (ICAO Doc. 7488)

Matías Gómez RO (2009). Volcanological map of the 1961–2009 eruption of Volcán de Pacaya, Guatemala. MS thesis, Michigan Technological University

Matías Gómez RO, Rose WI, Palma JL, Escobar-Wolf R (2012). Notes on a map of the 1961–2010 eruptions of Volcán de Pacaya, Guatemala. Geol Soc Am Digital Map Chart Series 10: 10 p

Melián, G., Hernández, P. a, Padrón, E., Pérez, N.M., Barrancos, J., Padilla, G., Dionis, S., Rodríguez, F., Calvo, D., Nolasco, D., 2014. Spatial and temporal variations of diffuse CO2 degassing at El Hierro volcanic system: Relation to the 2011-2012 submarine eruption. J. Geophys. Res. 119, 6976–6991. doi:10.1002/2014JB011013.Received

Métaxian, J. P., P. Lesage, and J. Dorel (1997), Permanent tremor of Masaya Volcano, Nicaragua: Wave field analysis and source location, J. Geophys. Res., 102, 22,529–22,545, doi:10.1029/97JB01141.

Mori, T., & Burton, M. (2006). The SO2 camera: A simple, fast and cheap method for ground-based imaging of SO2 in volcanic plumes. Geophysical research letters, 33(24).

Nadeau, P. A., Palma, J. L., & Waite, G. P. (2011). Linking volcanic tremor, degassing, and eruption dynamics via SO2 imaging. *Geophysical Research Letters*, *38*(1).

Nadeau, P. A. (2011). Ultraviolet digital imaging of volcanic plumes: implementation and application to magmatic processes at basaltic volcanoes.

Notsu, K., Mori, T., Do Vale, S.C., Kagi, H., Ito, T. (2006). Monitoring quiescent volcanoes by diffuse CO2 degassing: Case study of Mt. Fuji, Japan. Pure Appl. Geophys. 163, 825–835. doi:10.1007/s00024-006-0051-0.

Padrón, E., Hernández, P. a., Toulkeridis, T., Pérez, N.M., Marrero, R., Melián, G., Virgili, G., Notsu, K. (2008). Diffuse CO2 emission rate from Pululahua and the lake-filled Cuicocha calderas, Ecuador. J. Volcanol. Geotherm. Res. 176, 163–169. doi:10.1016/j.jvolgeores.2007.11.023.

Palma, J. L., E. S. Calder, D. Basualto, S. Blake, and D. A. Rothery (2008),Correlations between SO2 flux, seismicity, and outgassing activity at theopen vent of Villarrica volcano, Chile, J. Geophys. Res., 113, B10201, doi:10.1029/2008JB005577.

Ranaldi, M. (2008). Studio delle emissioni di gas in aree vulcaniche e geotermiche: implicazioni strutturali, geotermiche e di pericolosità.

Ripepe, M., and E. Gordeev (1999), Gas bubble dynamics model for shallow volcanic tremor at Stromboli, J. Geophys. Res., 104, 10,639–10,654, doi:10.1029/98JB02734.

Rissmann, C., B. Christenson, C. Werner, M. Leybourne, J. Cole, and D. Gravley (2012), Surface heat flow and CO2 emissions within the Ohaaki hydrothermal field, Taupo Volcanic Zone, New Zealand, Appl. Geochem., 27, 223-239.

Salazar, J. M., Hernández, P. A., Pérez, N. M., Melián, G., Álvarez, J., Segura, F., & Notsu, K. (2001). Diffuse emission of carbon dioxide from Cerro Negro volcano, Nicaragua, Central America. Geophysical research letters, 28(22), 4275-4278.

Schaefer, L.N., Oommen, T., Corazzato, C., Tibaldi, A., Escobar-Wolf, R., and Rose, W.I. (2013). An integrated fi eld-numerical approach to assess slope stability hazards at volcanoes: The example of Pacaya, Guatemala: Bulletin of Volcanology, v. 75, p. 720–738, doi:10.1007/s00445-013-0720-7.

Tamburello, G., Aiuppa, A., Kantzas, E. P., McGonigle, A. J. S., & Ripepe, M. (2012). Passive vs. active degassing modes at an open-vent volcano (Stromboli, Italy). Earth and Planetary Science Letters, 359, 106-116.

Verbovsek, T., 2011. A comparison of parameters below the limit of detection in geochemical analyses by substitution methods. RMZ - Mater. Geoenvirontment 58, 393–404.

Wardman, J., Sword-Daniels, V., Stewart, C., and Wilson, T. (2012). Impact Assessment of the May 2010 Eruption of Pacaya Volcano, Guatemala: GNS (Institute of Geological and Nuclear Sciences) Science Report 2012/09, 90 p.

WI Rose, JL Palma, R Escobar Wolf, RO Matías: (2013). 50 Years of Activity at a basaltic composite cone: Pacaya, Guatemala, 1961-2011 GSA Special Paper 498 “Open Vent Volcanoes” doi:10.1130/2013.2498(00)

Wunderman, R.L., and Rose, W.I. (1984). Amatitlán, an actively resurging cauldron 10 km south of Guatemala City: Journal of Geophysical Research, v. 89, p. 8525–8539, doi:10.1029/JB089iB10p08525.

11) Appendix

Table 2- Meteorological data from 1990 to 2012 from the station "Insivumeh" (data source: INSIVUMEH's website)

Wind Speed (Km/h)													
	Jan	Feb	Mar	Apr	May	Jun	Jul	Aug	Sep	Oct	Nov	Dec	Ave
1990	14,3	6	0	*N/D*	*N/D*	*N/D*	*N/D*	*N/D*	*N/D*	*N/D*	*N/D*	*N/D*	N/D
1991	4	3	13,7	11,9	11,4	9,7	15,1	13,9	12	11	16,8	16,6	11,6
1992	2	2,8	3,8	3,2	3,8	3,4	5,6	4,6	4	2,9	3,1	6	3,8
1993	8,1	5,5	5	3,6	2,3	2,,8	6,9	5,1	5,1	5,1	7,1	5,6	5
1994	7,1	6,6	2	5,7	6,6	7,1	8,3	11,6	7,1	6,4	6,7	5,1	6,7
1995	7	8	8	9,6	6,4	8,1	8,6	6,5	7,3	6,8	1,5	2	6,7
1996	3	4	4	4,6	5,6	4,3	4,2	5,4	6,2	5,3	*N/D*	7	4,5
1997	5	6,4	5	5,2	4,9	3,5	7,4	6,7	3,6	4,9	5,4	4,4	5,2
1998	5,6	7,2	6,7	5	4,8	4,5	5,1	5	3,6	4,1	6,5	6,9	5,4
1999	6,5	6	6,3	5,4	5,6	3	5,1	3,7	3	4	7,3	7,8	5,3
2000	6,9	6,5	4,7	5	3,4	4	5,9	5,3	2,9	6	5,1	7,3	5,3
2001	7,2	7,1	5,6	5,6	3,6	4,7	4,9	5,4	4,4	5,6	5,9	5,8	5,5
2002	6,4	6,2	11,9	5,7	8,2	3,7	5,3	5,8	4,7	4,2	5,9	5,2	6,1
2003	6,9	8,8	5	4,3	2,7	5,4	6,1	5	2,6	3,1	7,2	6,6	5,3
2004	7	5,8	8,2	5,7	11,4	4,9	12,3	11,6	7	6,6	12,7	13,3	8,9
2005	15,1	14,1	17,4	18,8	13,9	12,1	14,3	15,1	16,2	17	21,7	19,7	16,3
2006	24,8	22,4	18,5	18,1	12,3	15,2	16,9	17,1	13,5	6,9	19,8	18,8	17
2007	6,9	5,3	5,6	7,6	7,9	4,4	4,6	4,1	4,4	4,3	7,7	5,7	5,7
2008	6,4	8,5	10,3	10,2	8,8	10	7,8	8,2	8,4	11,6	23,5	21,9	11,3
2009	10	13,7	11,3	9,8	9,1	7,8	11,1	10,7	8,4	8,4	10,8	9,8	10,1
2010	12,6	11,4	11,1	10	9,7	9,7	9,7	8,5	7,7	8	7,8	9,6	9,7
2011	9,3	8,3	9,8	8,4	7,4	4,8	4,9	4,5	5,9	6,4	7,9	8,6	7,2
2012	8,8	7,9	8,6	7,1	5,2	5	5	5,7	11,7	15,9	22,7	19,2	10,2
Rainfall (mm/m)													
	Jan	Feb	Mar	Apr	May	Jun	Jul	Aug	Sep	Oct	Nov	Dec	Tot
1990	4,5	0,4	0,7	21,9	190,6	205,6	156,6	64,1	242,6	58,5	46,2	6,6	998,3
1991	4,6	0,8	0	14,4	128,9	328,6	157,6	68,3	180,8	189,7	161	51,8	1286,5
1992	1,5	0	11,7	32,5	21,9	261,3	189,2	210,5	151,5	134	21,8	0,6	1036,5
1993	0,1	0	11,4	97,4	65,3	300,4	110,4	233,9	229	112,9	29,5	0,2	1190,5
1994	5	0,4	0,9	12,5	122	170	125	256,8	188	101,2	3,3	3,1	988,2
1995	0,2	0,8	3,4	72,6	114,4	325,9	217,9	237,5	396,3	120	25,2	9,5	1523,7
1996	14,4	2	2,3	80,9	105,3	228,5	184,1	111,6	339,9	134,4	20,6	4,4	1228,4
1997	10,6	10,7	2,1	13,4	58,9	170,6	148,2	254,6	91,4	130,9	37	12,3	940,7
1998	0,1	0	21,2	0	68,9	280,1	216,9	210,6	127,6	224	355,5	3,6	1508,5
1999	1	52,2	0,4	6,4	96,8	295,1	277,8	221,7	326,9	174,3	19,7	3	1475,3
2000	0,4	0	0,2	40,9	231,4	306	62,1	130,4	220,2	41,5	14,5	1,6	1049,2

2001	1,1	4,8	2,6	4,1	129,5	162,8	175,1	223,3	152,7	137,6	19,6	1,3	1014,5
2002	0	6,6	0	12,7	76,4	208,4	163,7	109,3	242,9	108,6	83,6	0,2	1012,4
2003	0,9	14,4	20,3	36,8	159,9	303,1	186,8	109,4	374,2	42,1	18,6	2	1268,5
2004	0,2	0,5	23,9	5,2	24,3	314,5	197,2	97,6	228,2	165,9	2,9	0,2	1060,6
2005	2	0	6,7	2,6	141,9	211,8	415,1	278,3	180,2	128,7	23	2,5	1392,8
2006	11,3	0,4	6,3	32,6	153,5	449,8	192,6	94,3	211,7	216,9	39,2	9,1	1417,7
2007	1,4	0	0,9	31,2	84,8	206,7	219,6	333	287	114,4	2,1	1,5	1282,6
2008	3,3	11,9	3,4	22,4	169,6	460,3	410,6	187,3	354,8	67,4	0	0	1691
2009	0	4	0	17,3	161	189,6	94,4	141,5	90,2	81,2	130,5	29,5	939,2
2010	0	1,3	0	108,2	427,4	376,9	317,4	470,8	342,9	26,8	6,4	0	2078,1
2011	0	7,2	13,4	15	102	223	238,6	414	247	385	14,2	1,5	1659,5
2012	3,2	5,3	5,1	40,9	135,8	165,5	121,1	397,5	128,9	71,9	3,2	1,1	1,079,5
Average Temperature (C°)													
	Jan	Feb	Mar	Apr	May	Jun	Jul	Aug	Sep	Oct	Nov	Dec	Ave
1990	17,6	18,2	19,2	20,6	21,4	20,6	20,4	20,5	20,1	19,8	18,6	18,2	19,6
1991	18,4	18,8	21	21,8	21,5	20,6	20,3	20,6	20,1	19,6	18,4	17,9	19,9
1992	18,8	19,1	20,6	20,7	20,7	20,4	19,7	20	19,6	19,5	19,6	18,2	19,7
1993	18,4	18,7	19,7	21,2	21,8	20,4	20,2	19,6	19,7	19,5	18,1	17,5	19,6
1994	17,5	18,8	19,5	20,5	20,8	19,7	20	19,4	19,3	20	19,6	18,5	19,5
1995	18	19,4	20,5	19,4	21,5	20,6	20,1	20,3	19,4	19	18,7	18,4	19,6
1996	17	18,2	18,9	20,8	20,5	20,1	19,5	19,9	20	19,8	18,5	18,4	19,3
1997	15,5	19,4	20,5	21,6	20,7	20,5	20	20,7	19,3	20	19,9	18,3	19,7
1998	19,8	20,3	20,7	22,2	22,5	20,3	20,9	20,8	19,6	21,5	19	18,1	20,5
1999	17,4	17,3	19,6	20,9	20,7	19	19	19,3	18,4	18,4	17,3	17,8	18,8
2000	*N/D*	*N/D*	*N/D*	*N/D*	*N/D*	*N/D*	*N/D*	*N/D*	*N/D*	*N/D*	*N/D*	*N/D*	*N/D*
2001	16,8	18,1	19,2	20,3	20,4	19,5	20,1	19,9	19,2	19	17,3	18,3	19
2002	17,3	18,6	18,6	19,8	20,3	20,1	21	19,6	18,9	18,5	17,1	17,9	19
2003	16,8	17,8	24,8	20,6	20,7	19,1	20,3	20	19,7	20,2	19,2	17,5	19,7
2004	18,5	18,6	20,1	20,6	19,7	20,3	19,7	20,2	19,3	19,8	18,7	18,2	19,5
2005	17,7	19,3	20,9	20,9	23	22,2	21,8	21,1	21,2	19,7	18,2	18,4	20,4
2006	18	20,8	19,3	21,6	20,5	20,1	20,3	20,7	20,2	20,4	18,1	19,2	19,9
2007	19,4	19,2	19,1	20,5	21,1	20,5	20,8	20,2	20,1	18,9	18,7	19,2	19,8
2008	17,6	18,6	18,6	21,2	20,1	20,2	19,8	25,6	19,6	19,5	18,6	17,9	19,8
2009	19	19	19	21,5	21,5	20,8	21,2	21	20,7	20,5	18,9	19,4	20,2
2010	17,8	19,4	19,5	21,2	20,9	20	20,3	19,8	19,7	18,9	18,4	16,5	19,4
2011	19	19,6	19,5	20,9	20,8	20,6	20,5	20,4	19,9	19,3	19,5	18,5	19,9
2012	18,3	19,7	20,2	21	21,7	20,5	21,2	20,9	20,7	20,7	18,6	19,4	20,2

Table 3 Correction factors [Manual of the ICAO Standard Atmosphere (ICAO Doc. 7488)].

Difference in elevation	A	B
0	0	1
50	1.14	1.00481
100	2.29	1.00966
150	3.43	1.01453
200	4.57	1.01943
250	5.71	1.02437
300	6.86	1.02932
350	8	1.03431
400	9.14	1.03933
450	10.29	1.04438
500	11.43	1.04945
550	12.57	1.05457
600	13.71	1.05971
650	14.86	1.06489
700	16	1.07009
750	17.14	1.07532
800	18.29	1.08058
850	19.43	1.08588
900	20.57	1.09122
950	21.71	1.09658
1000	22.86	1.10198

Permissions:

- **Figures number 1, 2, 8 and 20** are pictures taken using Google Earth Pro and then modified in order to meet the needs of this work. The use of these pictures follows the rules and meets the policy of Google about the use of Google Maps and Google Earth Content. These conditions are published at the following link: https://www.google.com/permissions/geoguidelines/attr-guide.html

- **Figure number 24** has been made by Rudiger Escobar Wolf (rpescoba@mtu.edu) that on Jul 14th has given to me the permission to use this image. In the next page is reported the email that he wrote to me:

Carlo Maria Prandi <cmprandi@mtu.edu> Jul 14
to Rudiger

Hi Rudi,

can I use the attached picture in my thesis? What should I put in the citation?

Thank you.

Carlo Maria Prandi
Graduate Student of Geology
Mobile: +393348601353
Email: carlomaria.prandi@gmail.com

Get a signature like this: Click here!

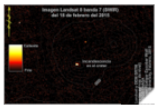

Rudiger Escobar Wolf <rpescoba@mtu.edu> Jul 14
to me

Sure, no problem. Just cite me as a personal communication (R. Escobar-Wolf, personal communication, July 2015).

If you need to prove that you have permission to use it (e. g. for the Grad School), you can use this email. I. e. Hereby I declare that I am the author of that image (using data cited in it) and I authorize you, Carlo Maria Prandi, to use the image in your master's thesis, and other publications you need it for.

Saludos: Rüdiger